The Thesis Committee for Svetlana Gennadiyevna Burris
Certifies that this is the approved version of the following thesis:

Gravity Studies over West Antarctica

APPROVED BY
SUPERVISING COMMITTEE:

Supervisor:

Donald D. Blankenship

Sean P. S. Gulick

Clark R. Wilson

Gravity Studies over West Antarctica

by

Svetlana Gennadiyevna Burris, B.S. Physics, B.S. Geology

Thesis

Presented to the Faculty of the Graduate School of

The University of Texas at Austin

in Partial Fulfillment

of the Requirements

for the Degree of

Master of Science in Geological Sciences

The University of Texas at Austin

December 2012

Acknowledgements

I would like to thank Duncan Young, Tom Richter, and Scott Kempf for all their help, expertise, and discussions. This thesis would not have been possible without their generous help and knowledge of all things gravity, data reduction, and code.

I would also like to thank my committee, Clark Wilson and Sean Gulick, for understanding and help along the way. Clark Wilson's classes in numerical methods and potential fields built my fundamental understanding behind this thesis.

My adviser, Don Blankenship, has been a tremendous supporter with his aid, guidance, understanding, and discussions.

And of course, I am thankful for the support and understanding of my husband, Brett Burris.

Abstract

Gravity Studies over West Antarctica

Svetlana Gennadiyevna Burris, MSGeoSci

The University of Texas at Austin, 2012

Supervisor: Donald D. Blankenship

This thesis describes the results of new analysis of gravity studies over West Antarctica. Set on the Siple Coast, an airborne geophysical survey was flown between 1994 and 1997 that covered the trunk of Bindschadler Ice Stream and the up-stream areas, including Whitmore Accommodation Zone and Byrd Subglacial Basin. The new gravity reduction methodology removed vertical and horizontal accelerations, the Eötvös effect, and the theoretical gravity; unlike previous analyses, this reduction did not level individual lines, preserving the high frequency data and avoiding introduction of new errors. This reduction provided the free-air gravity disturbance over the area, which was then leveled and registered by the more regional extensive GOCE satellite gravity. The processing and reduction of the data improved the high frequency signal over previous work on the data, giving better definition of small scale, short wavelength features, which

works well with satellite gravity data that emphasizes the large scale, long wavelength features. The leveled free-air gravity was then processed with a FORTRAN 90 program that calculates the Bouguer disturbance based on the free-air gravity and the topography. The topography was gathered concurrently with the gravity with ice penetrating radar during the airborne survey. The Bouguer disturbances provide a crustal model of the area. The final Bouguer disturbance was also corrected for the ice above sea level, which was calculated with a simple Bouguer slab correction. Finally, a power spectrum analysis was run on a profile in the Bouguer gravity disturbance in order to complete a spectral analysis. The spectral analysis provides crustal density boundaries for a density anomaly near the surface, a mid-crustal anomaly, and the Moho boundary. The improved the high frequency content of the data allows spectral analysis down to 4 km. The differing crustal thickness from spectral analysis also shows the character and extent of the West Antarctic Rift System, the northern flank of which extends out from Marie Byrd Land and into the survey area. Bindschadler Ice Stream is located on the WARS rift floor and MacAyeal Ice Stream sits on the rift flank.

Table of Contents

List of Tables

List of Figures

Chapter 1

Introduction

The slowly flowing West Antarctic Ice Sheet is buffered from oceanic influences by a series of fast flowing ice streams. Unlike the ice sheet, which is affixed to the underlying bedrock, ice streams flow relatively easily over the bedrock due to a thawed ice-bed, high-pressure basal water and underlying soft sedimentary beds. A sedimentary bed aids ice stream flow due to its low frictional resistance, and its ability to deform and create topography-smoothing till through erosion. (Alley et al., 1986, 1987; Blankenship et al., 1986, 1987, 2001; Rooney et al., 1987; Peters et al., 2006; Siegert et al., 2005) Such sediment-filled basins have been identified through seismic investigations of West Antarctic ice streams (Rooney et al., 1991; Anandakrishnan et al., 1998, 2003). Aerogeophysical observations over ice streams have been used to construct layered models of the crust beneath them from gravity and magnetic data, with a top sediment layer (Bell et al., 1998, 2006; Jordan et al., 2009). Seismic reflection and refraction observations have been made at the onset of Bindschadler Ice Stream which also indicate the presence of layered sediments in the basin beneath it (Peters et al., 2006). The top layer is interpreted to be a till-water system overlying three sedimentary layers which become more lithified with depth. Borehole observations also show a till-water and water conduit system (Kamb et al., 2001). Analysis of aeromagnetic data collected over

Bindschadler Ice Stream (Bell et al., 2006) also points to an underlying sedimentary basin, the southern end of which correlates to that located by seismic studies.

1.1 Research Objective

The goals of this research include better processing and analysis of original gravity data collected over Bindschadler Ice Stream, leveling airborne gravity with satellite gravity observations, calculating the Bouguer anomaly to better characterize the crustal gravity signal, and analyzing the frequency spectrum of Bouguer gravity to infer lithospheric structure beneath Bindschadler Ice Stream. The processing and reduction of the airborne data described here improves the high frequency signal content over previous analyses of the original data (Childers et al., 1999; Bell et al., 1999; Diehl et al., 2008), giving better definition of small scale, short wavelength features, which complements satellite gravity data which emphasizes large scale, long wavelength features. The crustal model of the area from analysis of the Bouguer disturbance is a necessary foundation for further work both to identify sedimentary basins beneath these ice streams and to understand the thermal evolution of the substantial rift system that underlies them.

1.2 Study Location and Methods

This work is based on airborne gravity data collected by the University of Texas at Austin Institute for Geophysics (UTIG) during three airborne geophysical field seasons, 1994-1995, 1995-1996, and 1996-1997, over West Antarctica's Ross Sea

Embayment. The data set consists of 110,000 line kilometers of aerogeophysical observations, spanning an area of about 200,000 km^2, which is somewhat larger than the state of Oklahoma. The survey area is divided into three main sections: Trunk D (TKD), Whitmore Accommodation Zone (WAZ), and the Byrd Subglacial Basin (BSB). These sections are made up of 12 blocks, which contain a total of 16 1^o by 1^o survey zones. The survey area encompasses a number of geologic features, including: the main trunk of Bindschadler Ice Stream, formally known as Ice Stream D; Bentley Subglacial Trench; Byrd Subglacial Basin; Siple Dome; and, subglacial volcanoes. The ice thickness in the area ranges from 200 m to 3900 m (Bell et al., 1999).

The airborne geophysical survey was conducted aboard a Twin Otter aircraft, which carried a suite of instruments, including a gravimeter, magnetometer, ice-penetrating radar, and laser altimeter as well as a Global Positioning System (GPS), inertial navigational system, and a pressure altimeter. There was also a base station with a magnetometer and GPS. The gravimeter used was a Bell Aerospace BGM-3 gravity meter (Bell et al., 1999).

1.3 Data Reduction and Analysis

To prepare the gravity data for analysis, it has undergone vertical and horizontal acceleration corrections, removal of theoretical gravity, and Eötvös corrections to account for gravity measured on a moving platform over a rotating planet. This reduction of the data was done with functions written in Matlab. The gravity lines, which were not explicitly leveled to one another, had spurious data trimmed off based on anomalous

cross-over errors and visual assessment of each block in its entirety. Often, poor data resulted at the beginning of a profile line, when the gravimeter was stabilizing following a turn by the aircraft.

The reduction of the data provides a map of free-air gravity disturbances, with overall errors within a particular season that are comparable to gravity produced by traditional analysis of the same data using relative line-leveling (Bell et al., 1999). Also, because corrections for horizontal accelerations are applied in the new analysis, high frequency content comparable with more recent field work is achieved (Richter et al., 2001; Holt et al., 2006). The separate sections are connected to each other with GOCE satellite gravity leveling. The satellite gravity, due to its high position above the earth, records long wavelength gravity signals, and vice versa for the airborne gravimeter. This geometry means that airborne gravity is best suited to examine short wavelength, high frequency signals or features, while satellite gravity is best suited for long wavelength, low frequency signals. Therefore, the newly leveled data can be studied for the crustal gravity signal, because the airborne gravity data set is connected to the regional gravity signal through leveling by the satellite gravity.

A 2D Bouguer disturbance was calculated using FA2BOUG, a FORTRAN 90 program (Fullea et al., 2008). The input gravity was the previously GOCE-leveled gravity. The output Bouguer disturbance has undergone Bullard A, B, and C corrections, and accounts for on-shore, i.e. above sea level, and off-shore, i.e. below sea level, points (Fullea et al., 2008). If the topography was below sea level, then the volume between the

topography and sea level was treated as ice, rather than water. The Bouguer disturbance was also then processed to remove a simple Bouguer slab that accounts for the overlying ice.

1.4 RESULTS

The results show significant free-air gravity disturbances associated with sub-ice topography upstream of Bindschadler Ice Stream, at Siple Dome, and over the Bentley Subglacial Trench. The free-air gravity provides a basis for calculation of Bouguer anomalies using bedrock topography from simultaneously collected ice penetrating radar. Using the spectral character of these Bouguer anomalies, interpretations can be made of the vertical structure of the lithosphere. These interpretations can be used to test hypotheses for evolution of the lithosphere beneath the ice streams; they also form a foundation for further work to calculate isostatic anomalies that can be used to establish geologic boundaries of sedimentary basins underlying the ice.

Chapter 2

Ross Sea Embayment

2.1 ANTARCTICA

The Antarctic continent is composed of two tectonic provinces: the Precambrian East Antarctic craton and the Mesozoic to Cenozoic West Antarctic craton (Dalziel, 1992). East Antarctica (EA) is cold, continental lithosphere, which ranges in thickness from approximately 220 km below Dronning Maud Land to 270 km below Wilkes Land (Morelli and Danesi, 2003); the crust itself was estimated at about 40 km thick from seismological studies (Roult and Rouland, 1994), but more recent work by Winberry and Anandakrishnan (2004) and Lawrence et al. (2006a,b) indicate a crustal thickness of 34 to 35 km. Teleseismic S-wave attenuation studies, which are non-unique, suggest that EA has thick, subcontinental lithosphere (>250 km), i.e. a continental root, which is underlain by a negligible thickness of asthenosphere (Lawrence et al., 2006b). Heat flux distribution over EA is similar to that over stable continents (Shapiro and Ritzwoller, 2004; Fox Maule et al., 2005; Llubes et al., 2006).

East and West Antarctica are separated by the Transantarctic Mountains (TAM). The TAM are a 3500-4000 km range that marks a change from the older, stable East Antarctic craton to the younger accreted terranes and rift system of West Antarctica

(Dalziel, 1992; Siddoway, 2008). The TAM are a 200 km wide and 4 km high mountain range (Lawrence et al., 2006b). The TAM are unique, as they are not formed due to collisional tectonism (ten Brink et al., 1997). There are a few theories for their formation: a broken plate or transform-flank uplift model, with uplift provided by thermal buoyancy due perturbed upper mantle temperatures (ten Brink et al, 1997); an isostatically buoyant load due to thicker crust (Studinger et al., 2004); and the collapse of a thick plateau, followed by denudation along the mountain front (Bialas et al., 2007). However, it is generally agreed that thermal buoyancy alone cannot account for the elevation of the TAM and that there need to be additional mechanisms (Studinger et al., 2004; Lawrence et al., 2006a). While the origin of the TAM is in question, a transition zone from the high velocity mantle in EA to the low velocity mantle in West Antarctica (WA), with a sharp contact below the TAM has been identified in surface wave (Morelli and Danesi, 2003) and heat flux studies (Shapiro and Ritzwoller, 2004). Seismic receiver functions also show a ~5 km thick crustal root beneath the mountain range, which is part of the maximum crustal thickness of ~40 km below the crest of the TAM (Lawrence et al., 2006a).

2.2 WEST ANTARCTICA

In contrast to the old East Antarctic craton and the thick crust on the TAM, WA is composed of five major sections: Antarctic Peninsula, Thurston Island, Ellsworth-Whitmore Mountains, Marie Byrd Land, and the West Antarctic Rift System (WARS) (Dalziel and Lawver, 2001). The first four are geologically distinct terranes (Dalziel and

Elliot, 1982) and are separated by subglacial depressions which generally follow the WARS (Jankowski and Drewry, 1981; Dalziel, 2006). The Antarctic Peninsula, Thurston Island, and Marie Byrd Land are Paleozoic to Mesozoic fore-arc and magmatic-arc terranes which developed along the Pacific margin of the Gondwana craton, specifically between South America and Australia, and accreted to the East Antarctic craton during the Phanerozoic (Dalziel, 1992). The Ellsworth-Whitmore Mountains block is a displaced segment of the craton margin, specifically the Pacific edge of East Antarctica (Schopf, 1969; Dalziel, 1992). All four crustal blocks of West Antarctica moved during Gondwanaland fragmentation between the Mid-Jurassic and the Cretaceous relative to each other and East Antarctica. During this fragmentation, there was extension between East Antarctica and the West Antarctic crustal blocks, which is supported by marine and airborne geophysics, and paleomagnetism. Paleomagnetic data and reconstructions of seafloor spreading establish the present geographic configuration of the Antarctic continent, when the New Zealand microcontinent separated from the Ross Sea – Marie Byrd Land margin, by the Late Cretaceous (Dalziel, 1992; Dalziel, 2006). This tectonism was not the end of spreading in West Antarctica, with interpretation of marine geophysical data from the Adare trough indicating up to 180 km of Neogene extension between East Antarctica and Marie Byrd Land (Cande et al., 2000). Volcanic activity in the area also indicates separation between East and West Antarctica during the late Mesozoic, Neogene, and Quaternary (Dalziel, 2006).

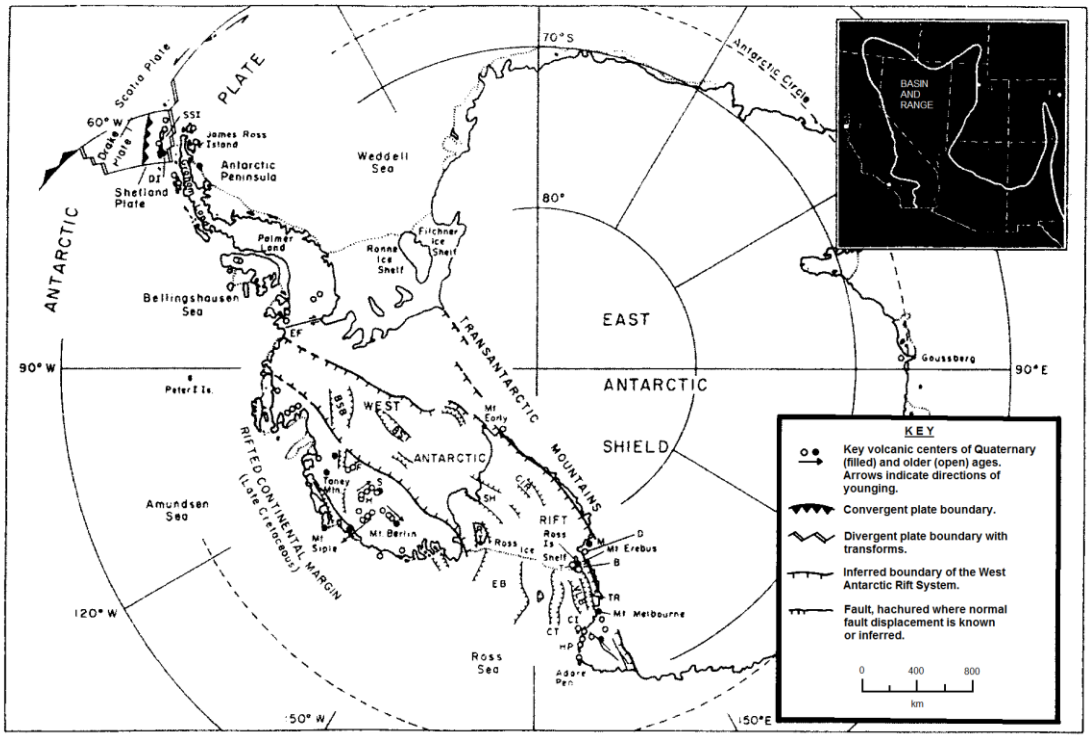

Figure 2.1: *The West Antarctic Rift System (WARS), abutted by the Transantarctic Mountains to the south. WARS contains the Byrd Subglacial Basin (BSB) and Bentley Subglacial Trench (BST). The Basin and Range province is outlined in the right hand corner, relative to the United States. (Figure from Dalziel, 2006; WARS from LeMasurier, 1990).*

The West Antarctic Rift System (WARS) begins along the most elevated region of the Transantarctic Mountains, with the southern margin continuing along the northwestern boundary of the Ellsworth-Whitmore Mountains (Figure 2.1); the northern boundary is usually defined along the inner edge of Marie Byrd Land (LeMasurier 1990; Luyendyk et al., 2003; Dalziel, 2006) or may incorporate Marie Byrd Land (Winberry

and Anandakrishnan, 2004). The asymmetrical rift along the southern edge is defined by a 3000 km long, 4-5 km high rift shoulder (Behrendt, 1999). It covers an area approximately the same size as the North American Basin and Range province, sweeping from the Ross Sea to the Antarctic Peninsula (Figure 2.1); at 3000 km in length and up to 1000 km wide, it is one of the largest continental rifts in the world (Achauer and Masson, 2002; Luyendyk et al., 2003). Seismic studies in Antarctica have measured crustal thickness (Figure 2.2), yielding results that show much thinner crust in West than East Antarctica; crust in West Antarctica is 21-31 km thick while craton crust in East Antarctica is 34 km thick (Winberry and Anandakrishnan, 2004). Bentley Subglacial Trench, located towards the middle of the WARS, has the thinnest crust in the West Antarctica at 21 km (Winberry and Anandakrishnan, 2004); the 100 km by 500 km trench reaches depths of 3 km below sea level, with greater than 0.5 km of sediment fill (Winberry and Anandakrishnan, 2004; Anandakrishnan and Winberry, 2004). Previous interpretations of extension during the Cretaceous to the middle Cenozoic in West Antarctica are reinforced by the observations of thin crust, which in turn highlights the full extent of the WARS, making it a major tectonic province in Antarctica (Bradshaw, 1989; Weaver et al., 1994; Luyendyk, 1995; Cande et al., 2000; Winberry and Anandakrishnan, 2004). At the Ross Sea and Ross Ice Shelf, the WARS becomes the Siple Coast.

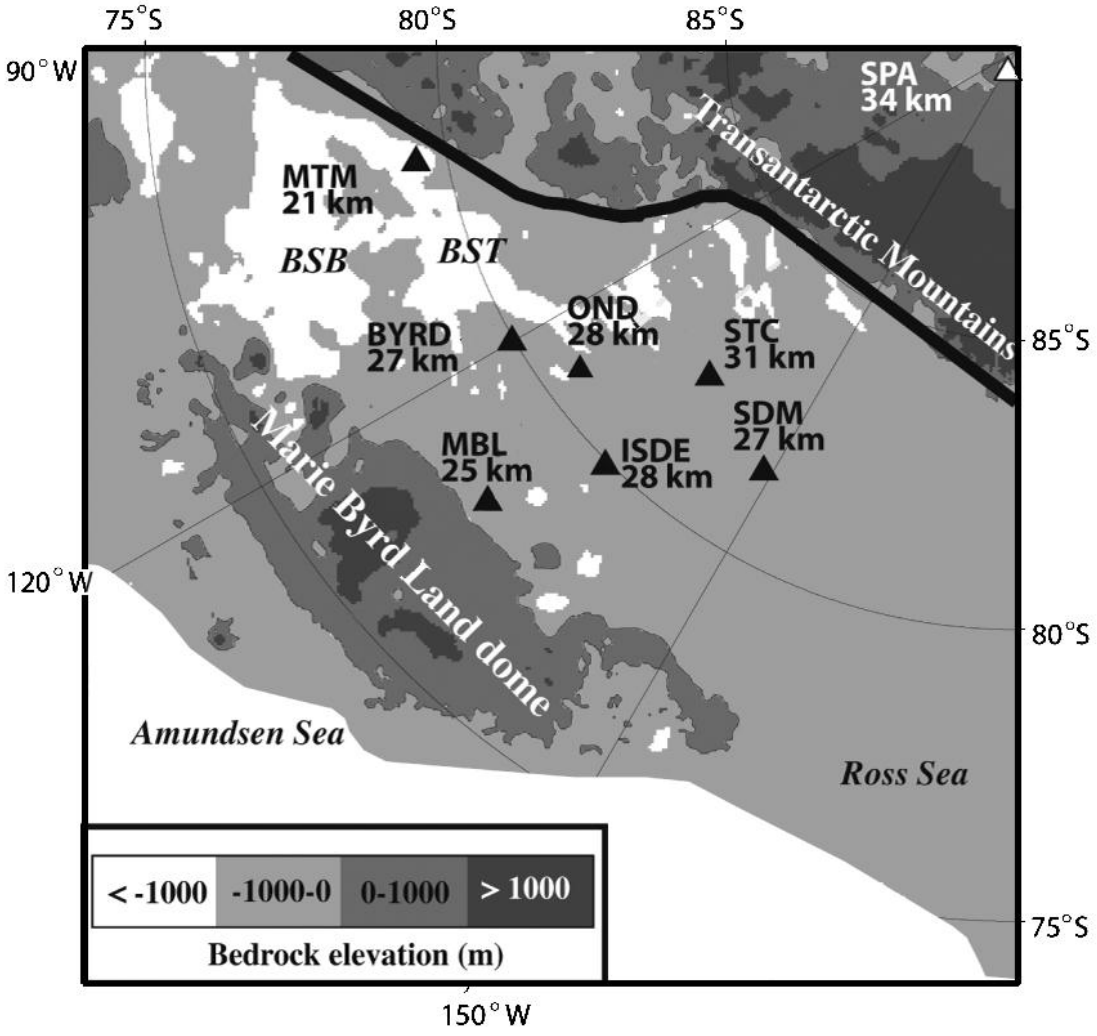

Figure 2.2: *Crustal thickness estimates given as measured from the base of the ice sheet. Black triangles indicate seismic stations, white triangle indicates the South Pole (SPA), thick black line indicates the approximate southern boundary of the West Antarctic Rift System, BSB – Byrd Subglacial Basin, and BST – Bentley Subglacial Trench. (Figure modified from Winberry and Anandakrishnan, 2004)*

2.3 SIPLE COAST AND THE ROSS SEA EMBAYMENT

The Siple Coast, at the western, continental edge of the West Antarctic Rift System, spans over 600 km from the Transantarctic Mountains to Marie Byrd Land. There are eleven major ice streams in West Antarctica, with five of these ice streams located on the Siple Coast, flowing into the Ross Ice Shelf. The five Siple Coast ice streams were originally named Ice Stream A – E, but have been renamed to Mercer Ice Stream (A), Whillans Ice Stream (B), Kamb Ice Stream (C), Bindschadler Ice Stream (D), and MacAyeal Ice Stream (E) (Figure 2.3). Nestled in between Kamb and Bindschadler Ice Streams is Siple Dome (Figure 2.3); Siple Dome stands approximately 400 m higher than the surrounding ice streams, acting as an interstream ridge, and it is a stable feature in the West Antarctic landscape (Hamilton, 2002). The Siple Coast ice streams have undergone significant changes over time: Kamb Ice Stream shut down approximately 130-150 years ago (Retzlaff and Bentley, 1993; Anandakrishnan and Alley, 1997; Jacobel et al., 2000); ice stream speeds have changed, with Whillans Ice Stream losing speed by 50% and overall velocity fields shifting in just this past century (Bindschadler and Vornberger, 1998); and, ice stream margins have migrated, especially with the shutdown of Kamb Ice Stream (Jacobel et al., 2000).

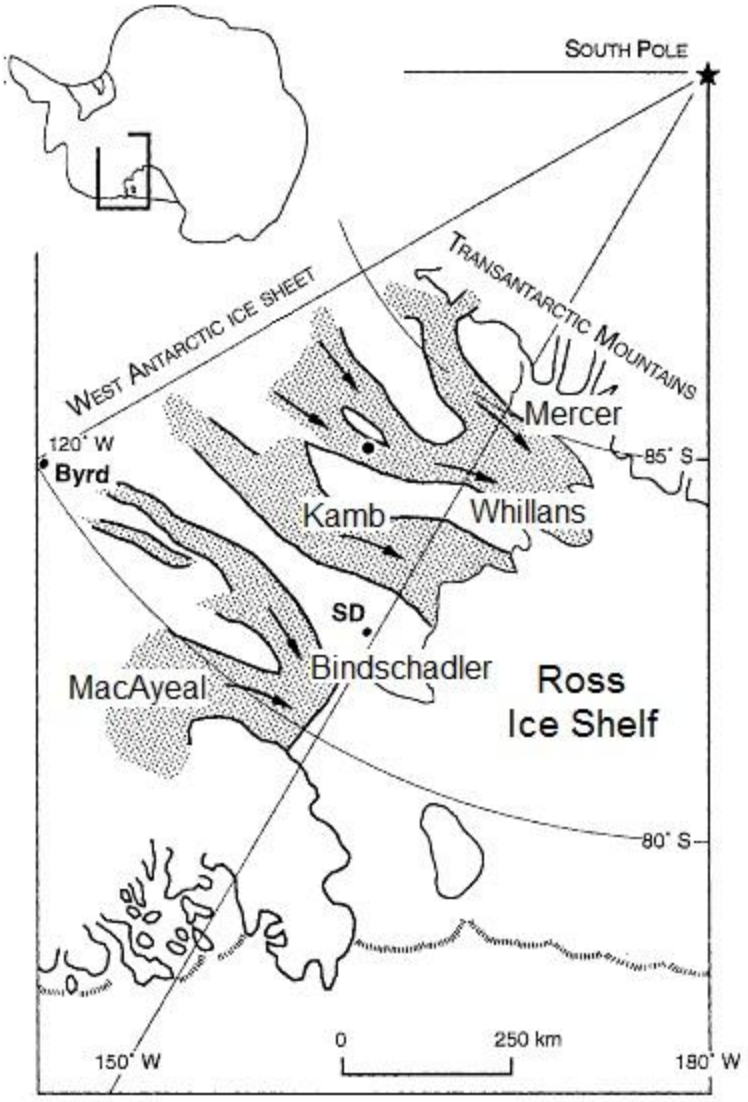

Figure 2.3: *Siple Coast with its five ice streams. SD marks the location of Siple Dome. (Figure modified from Engelhardt, 2004)*

The Ross Sea Embayment, composed of the Ross Ice Shelf and the Ross Sea (Figure 2.1), defines part of the boundary between East and West Antarctica. The

Embayment contains the Ross Sea rift within its subsided crust (LeMasurier and Rex, 1990; Tessensohn and Worner, 1991; Storey et al., 1999). The Ross Sea rift, which is a passive rift, results from stretching of the lithosphere during an early phase (Cretaceous), followed by a second phase (Cenozoic) of delayed asthenospheric upflow (Sengör and Burke, 1978; Tessensohn and Worner, 1991; Cande et al., 2000). The first phase is characterized by lack of volcanism and diffuse crustal attenuation, with several offshore basins in-filling with sediments, including Victoria Land Basin and faults on Iselin Basin (Cooper and Davey, 1987; Tessensohn and Worner, 1991). The second phase was brought up by Gondwanan rifting, with uplifting and tilting of the Transantarctic Mountains, asymmetric subsidence of the rift, especially in the Victoria Land Basin, and onset of volcanism in the mid-Cenozoic (Fitzgerald et al., 1987; Tessensohn and Worner, 1991; Luyendyk et al., 2003).

2.4 ICE STREAMS

There are five ice streams along the Siple Coast. Ice streams are defined as "a region in a grounded ice sheet in which the ice flows much faster than in regions on either side" (Paterson, 1994). Ice streams make up the most dynamic components of contemporary ice sheets, displaying changing spatial and temporal behavior (Retzlaff and Bentley, 1993; Anandakrishnan and Alley, 1997; Bindschadler and Vornberger, 1998; Jacobel et al., 2000; Stokes and Clark, 2001; Truffer and Echelmeyer, 2003; Ng and Conway, 2004). There are a range of ice stream flow mechanisms, from deep, narrow channels, such as Jakobshavn Isbrae in Greenland, to shallow, broad ice streams that

dominate West Antarctica (McIntyre, 1985; Bentley, 1987; Truffer and Echelmeyer, 2003). These shallow, Siple Coast ice streams, or their onset areas, on the Siple coast are typically underlain by a layer of saturated sediment (Blankenship et al., 1986; Blankenship et al., 1987; Engelhardt et al., 1990; Rooney et al., 1991a; Smith, 1997; Anandakrishnan et al., 1998; Bell et al., 1998; Blankenship et al., 2001; Doake et al., 2001; Studinger et al., 2001; Anandakrishnan, 2003; Vaughan et al., 2003; Peters et al., 2006). From comparisons of ice streams from West and East Antarctic, Greenland, and the Laurentide/Cordilleran ice sheets, the Siple Coast ice streams are characterized by their slippery beds, low driving stresses, and support from their narrow shear margins (Truffer and Echelmeyer, 2003).

The till-water system below ice streams aids them in their flow due to their lubricative and dilatant properties: water saturated sediments make up the till, which deforms due to dilation of the grains, lessens the bed roughness, and thereby lubricates the ice stream bed (Blankenship et al., 1986, 1987; Alley et al., 1986, 1987; Alley, 1993; Anandakrishnan et al., 1998; Bell et al., 1998; Blankenship et al., 2001; Studinger et al., 2001; Anandakrishnan et al., 2003; Siegert et al., 2004; Siegert et al., 2005). Modeling and seismic observations suggest that the till-water system is underlain by a soft sediment bed, possibly becoming more lithified towards the bedrock (Engelhardt et al., 1990; Tulaczyk et al., 1998; Anandakrishnan et al., 2003; Peters et al., 2006). The soft sediment bed allows more rapid basal motion (Engelhardt and Kamb, 1998; Kamb, 2001; Peters et al., 2006), with fast ice flow initiated and maintained through abundant, high-pressure

basal water (Blankenship et al., 1986; Alley et al., 1994; Anandakrishnan and Alley, 1997). The inland extent of the ice stream flow also appears to be determined by the extent of the underlying sediments (Anandakrishnan et al., 1998; Bell et al., 1998; Blankenship et al., 2001; Studinger et al., 2001). Bed roughness may influence ice stream velocities through tractional processes, like 'sticky spots' (Alley, 1993), strain heating (Hättestrand and Stroeven, 2002), and hydrological organization (Hindmarsh, 1998). The resulting difference in velocity between the ice streams and the ice sheet is on the order of 10^2-10^3 m/year versus ~10 m/year.

In addition to transporting ice from the ice sheet, ice streams also impact the ice transport process through their spatial and temporal changes (McIntyre, 1985; Shabtaie et al., 1988; Joughin et al., 2002; Joughin and Tulaczyk, 2002; Bindschadler et al., 2012). Rapid sea level rise has been postulated if flow acceleration of the West Antarctic Ice Sheet occurs (Hughes, 1977), so it is the stability of ice streams that becomes vital in determining the rate and direction of ice volume change in the ice sheet, more so than just inland ice accumulation rates (Whillans and van der Veen, 1993; Schoof, 2001).

Chapter 3

Free-Air Gravity Disturbances

3.1 THEORY

As the Earth is not a perfect sphere, there are several ways to define gravity. Technically, the truest way to define the gravity anomaly vector is by subtracting the normal, i.e. perpendicular, gravity on the reference spheroid from the gravity at the geoid, as the spheroid and geoid do not coincide (Hackney and Featherstone, 2001). The geoid is the equipotential gravity surface of the Earth, while the spheroid is the oblate spherical approximation of the Earth's shape. A gravity disturbance is calculated by subtracting the normal gravity at the measurement point from the observed data; the normal gravity at the measurement point is the gravity on the reference spheroid with free-air and Bouguer corrections (Hackney and Featherstone, 2001). As the goal in geophysical applications is to examine a specific locality, it is important to remove the extraneous, surrounding effects, like the mass of the Earth and other large-scale gravity effects (LaFehr, 1991a; Hackney and Featherstone, 2001). For geological studies, gravity disturbances and anomalies can be used to define structure, densities, and crustal boundaries (Hackney and Featherstone, 2001; Tenzer et al., 2008). The formula for gravity is based on latitude (θ), height, and longitude (ϕ), upon which it has no dependence; it is a scalar field in three

dimensions and the first derivative of potential *(U)*, however, two of its vectors are zero at the Earth's surface:

$$\vec{g} = \frac{d}{ds} U(\phi, \theta, h)$$

The free-air gravity disturbance for airborne gravity is calculated by removing: the theoretical gravity based on an ellipsoid; the acceleration due to the Earth's rotation, i.e. the Eötvös effect; the vertical and horizontal accelerations due to aircraft motion; and, the free-air gravity correction.

3.2 DATA

This work is based on airborne gravity data collected by the University of Texas at Austin Institute for Geophysics (UTIG) during three airborne geophysical field seasons, 1994-1997, over West Antarctica's Ross Sea Embayment, specifically areas in the Siple Coast. The airborne geophysical survey was conducted aboard a Twin Otter aircraft, which carried a suite of instruments, including a gravimeter, magnetometer, ice-penetrating radar, Global Positioning System (GPS), laser altimeter, inertial navigational system, and a pressure altimeter. There was also a base station with a magnetometer and GPS. The data set consists of 110,000 line kilometers which span an area of 200,000 km^2, an area that is only somewhat larger than the state of Oklahoma.

The choice of an airborne survey is advantageous due to the freedom of survey design – no geographical, environmental, national, or topographical restraints – and freedom of increased sampling rates – aircraft travel faster than snowmobiles over

crevassed regions. Airborne surveys are not restricted by terrain or access roads, and they can be designed to target the scientific question by selecting the appropriate survey line intervals. The aircraft also functions as a platform for multiple instruments much more readily than a snowmobile would.

3.2.1 Location

The survey area is divided into three main sections: Trunk D (TKD), Whitmore Accommodation Zone (WAZ), and Byrd Subglacial Basin (BSB) (Figure 3.1). These sections are made up of 12 blocks, which contain a total of 16 1^o by 1^o survey zones. The survey area encompasses a number of geologic features, including: the main trunk of Bindschadler Ice Stream, formally known as Ice Stream D; Bentley Subglacial Trench; Byrd Subglacial Basin; and Siple Dome. The ice thickness in the area ranges from 200 m to 3900 m (Bell et al., 1999).

The flight pattern formed an orthogonal grid, with line spacing of 5.3 km in both directions, which gives about 400 cross-overs in each survey zone. The cross-overs help identify discrepancies between lines and lines with less-than-valid data. The elevation in each individual survey zone was constant, but could differ between zones. The differing elevation results from accommodation of the laser altimeter, which can only range the surface in cloud-free conditions.

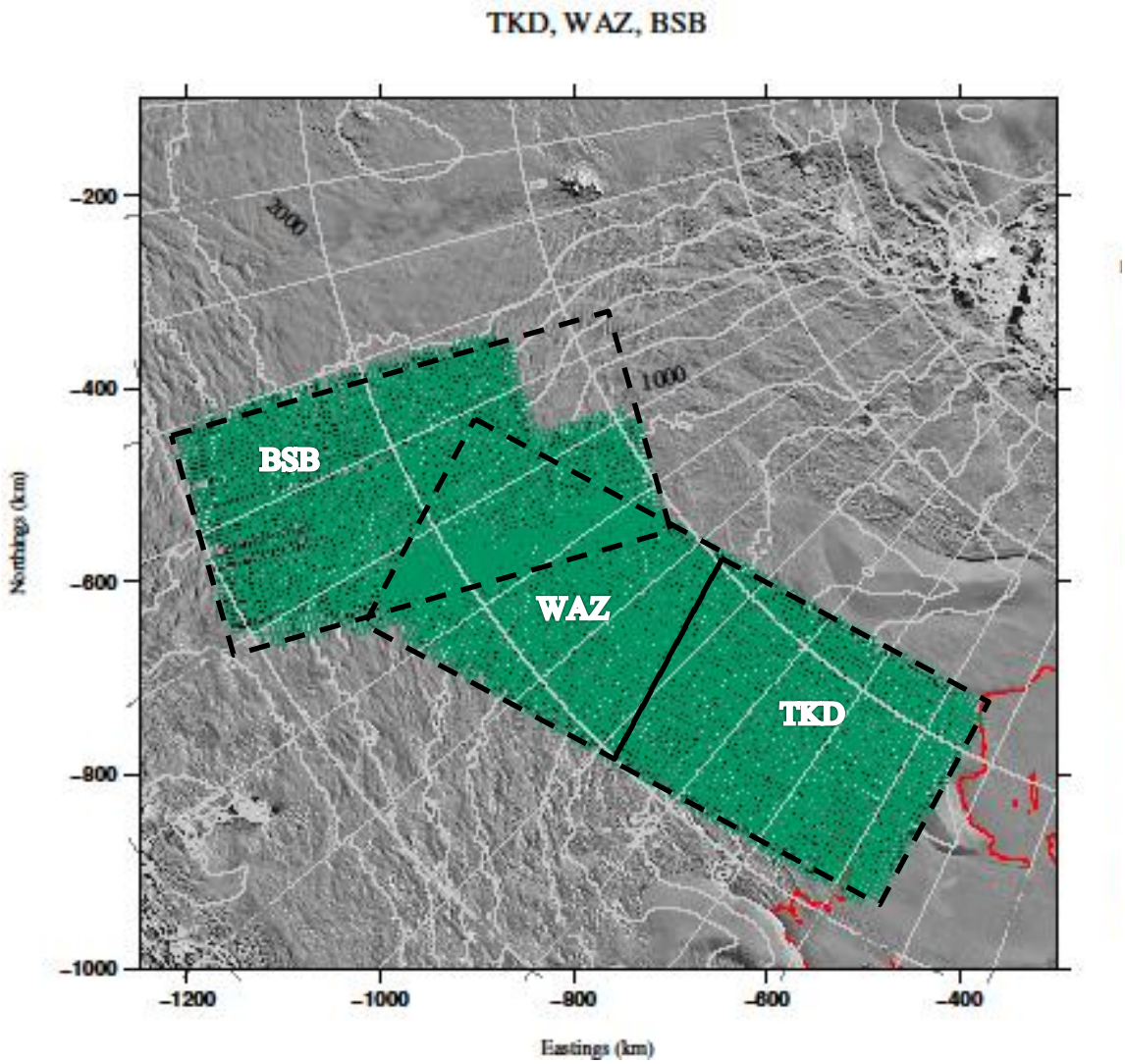

Figure 3.1: *The location of the survey area on the Siple Coast. Black dashed lines outline the sections. This and all plots were made with Generic Mapping Tools (GMT). Overlap is exaggerated.*

3.2.2 Instruments

The gravimeter used was a Bell Aerospace BGM-3 gravity meter. The magnetometer was a proton-precession magnetometer (a Geometrics 813), which takes measurements every 60 m, with an estimated precision of 1 nT, and the base station magnetometer was used to monitor the changing magnetic field and to remove the diurnal magnetic signal. The ice penetrating radar used was developed by the National Science Foundation and the Technical University of Denmark in the 1970s and upgraded to a digital system by UTIG working with the United States Geological Survery (USGS) (Blankenship et al., 2001); it operates on a carrier frequency of 60 MHz, with a peak transmission power of 10 kW, to penetrate over 4 km of ice (Skou and Sondergaard, 1976). The GPS system consisted of real-time differential GPS navigation, a GPS/GLONASS receiver, and a suite of carrier phase GPS receivers. The Holometrix Pram IV laser altimeter has a ranging accuracy of 0.1 m, collects data every 10 m, and has a footprint of 0.9 m. The inertial navigational system was a Litton 92, which measured three components of acceleration as well as the pitch and roll angles of the plane that were used to correct laser ranges for off-nadir aircraft attitudes.

The BGM-3 (Figure 3.2) is based on a proof mass that is held in place electromagnetically that measures vertical accelerations with feedback circuits (Bell Aerospace, 1979). A two-axis gyroscope stabilizes the vertical acceleration sensor on short timescales, while on longer timescales a platform erection system attempts to align the sensor with vertical (Bell Aerospace, 1979). The gravity meter was sampled at 1 Hz.

The gravity meter records relative gravity requiring that the meter be tied to an absolute gravity datum in order to give an absolute gravity reading. For this data set, the airborne gravity measurements were tied to absolute gravity stations in Antarctica through a closed loop with a handheld gravity meter.

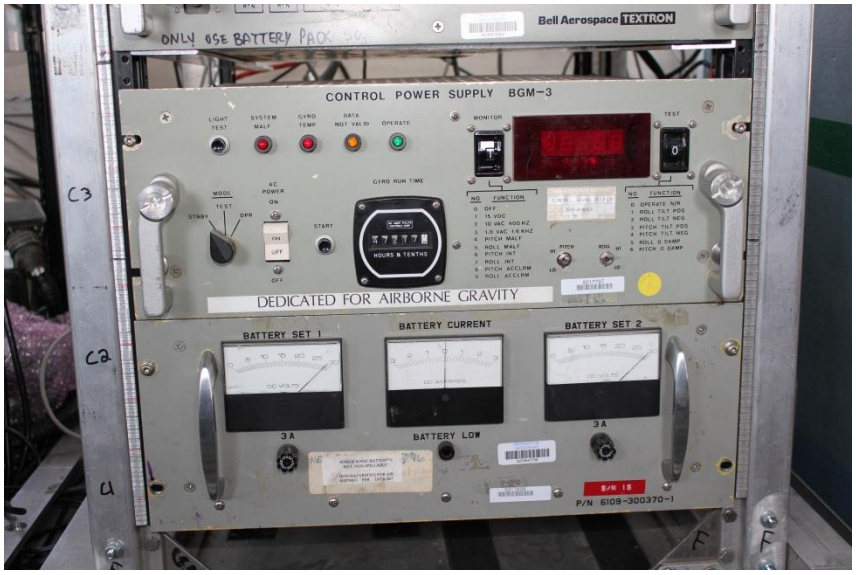

Figure 3.2: *The front of the BGM-3 gravity meter, as installed on an aircraft rack.*

3.3 DATA REDUCTION

The reduction process was done with Matlab code written by Tom Richter at UTIG; part of the process is described in Richter et al. (2001) and Holt et al. (2006). It takes in the raw data from the gravity meter, maps it with the concurrently collected GPS data, and puts out a file with the year, day, time, longitude and latitude in Cartesian coordinates, and the gravity disturbance in milli-Gal (mGal). The data was also either

adjusted forward or backward in time in order to account for any misalignment between the gravity and GPS time stamps.

3.3.1 Horizontal and vertical accelerations

The first correction applied in the code is for the horizontal and vertical accelerations of the aircraft. Vertical accelerations are from the aircraft moving up or down, e.g. when gaining altitude, while horizontal accelerations are due to aircraft movement side to side relative to the track. The vertical acceleration is found by double differencing the measured gravity; after conversion to mGal, this is the vertical acceleration of the GPS. The horizontal accelerations are found using the length of the latitude and longitude, based on the axis of the World Geodetic Surface of 1984 (WGS-84) ellipsoid, and the average GPS velocities. The along track and across track velocities are also calculated assuming a spherical Earth, the errors of which are below the threshold of the analysis. Tilt, both pitch and roll, of the gravity meter is also accounted for by calculating the angular frequency based on the pitch period, taking into account the along track GPS accelerations. The roll is calculated in a similar manner by using the angular frequency based on the roll period and the across track accelerations.

3.3.2 Eötvös

The code then calculates the acceleration due to the Earth's rotation, i.e. the Eötvös effect (Harlan, 1968). The input vectors are latitude, longitude, and height relative

to WGS-84, and the velocity north and east vectors, which are the aircraft ground speed, i.e. the track over the ground. The Eötvös correction is:

$$E\ddot{o}tv\ddot{o}s = 2v_E\omega\cos\theta\left(1+\frac{h}{a}\right)+\frac{v_N^2}{a}\left(1+\frac{h}{a}+f\,(2-3\sin(\theta)^2)\right)$$

$$+\frac{v_E^2}{a}\left(1+\frac{h}{a}-f\sin(\theta)^2\right)$$

where v_E is velocity east, v_N is velocity north, ω is the angular speed of the Earth, θ is the latitude, h is the height above WGS-84 datum, a is the semi-major axis of the WGS-84 ellipsoid, and f is the geometric flattening of the WGS-84 ellipsoid.

3.3.3 Theoretical Gravity:

The theoretical gravity is calculated at sea level relative to the spheroid using the closed form from Featherstone (1995):

$$g = g_{En}\left(1+\frac{k\sin(\theta)^2}{\sqrt{1-e\sin(\theta)^2}}\right)$$

where $g_{En}$is the normal gravity at the equator for WGS-84, k is the normal gravity constant for WGS-84, θ is the latitude, and e is the first numerical eccentricity for WGS-84. The second-order free air correction is applied from Li and Götze (2001) for Geodetic Reference System 1980 (GRS-80). As both the free-air and Eötvös corrections bring the gravity to sea level, those corrections were added, leaving theoretical gravity to be subtracted from the observed gravity.

3.3.4 Final corrections

At this point, due to the nature of the BGM-3 electric circuit, the second derivative of the height with respect to time is convolved with gravity signal fall off, which is based on the physical resistor-capacitor circuit ($e^{-\frac{1}{RC}}$), which leaves low-pass filtered results. It functions as an infinite pulse response system. Finally, the gravity is filtered with a kernel smoother which is based on the Epanechnikov kernel (Epanechnikov, 1969).

Once the gravity has been reduced, the gravity profile lines are gridded, plotted, and edited. The gravity meter does not react well to sudden changes or extreme, relatively speaking, angles. The gravity meter gyroscopes need time to settle out, especially when coming out of a turn at the beginning of a line. Bad sections of data can also be due to jumps in GPS or turbulence. Using that information, visual analysis of the plotted data, and the cross-over error at intersections of lines, the total root-mean-square (RMS) of each zone was reduced by, usually, trimming the beginning of a line. Some very obviously noisy lines were removed all together.

3.4 ERROR

Previous analysis of this data set produced a minimal RMS of 2.98 after "significant editing" and local leveling of intersecting lines within a survey zone, but without correction for horizontal accelerations (Bell et al., 1999). In this analysis, out of 12 blocks, 6 blocks had an improved RMS, especially in TKD and WAZ, and 4 blocks were comparable, especially in BSB (Table 3.1). The two blocks in BSB that show larger

RMS values, C and N, were flown over two seasons. Instrument drift, which varies from season to season is not removed without leveling individual lines, which was not done for this analysis. The absence of local line leveling is in the contrast to the previous analysis (Bell et al., 1999), and the RMS values still hold up well against the 2.98 mGal RMS achieved then. The histograms show the cross-over values (Figure 3.3), which tend to cluster around the average RMS shown for each block in Table 3.1.

Table 3.1: *The average RMS in mGal for each block.*

TKD		**WAZ**		**BSB**	
C	2.58	NE	2.86	C	7.38
NE	2.08	NW	2.91	N	8.35
SE	2.93	SW	3.41	SC	3.22
W	2.48			WC	3.10
				W	3.39

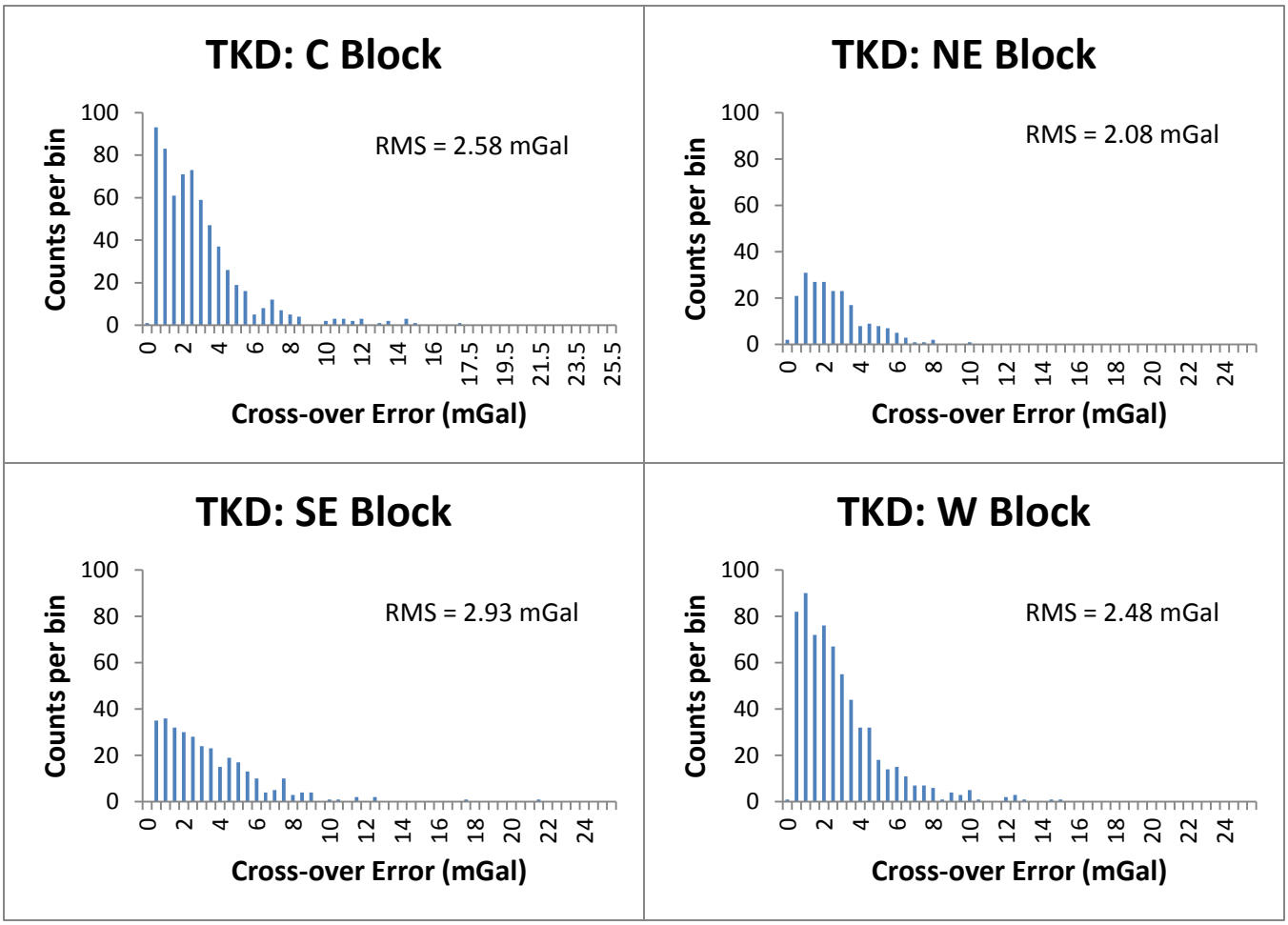

Figure 3.3a: *The histograms for the TKD Blocks.*

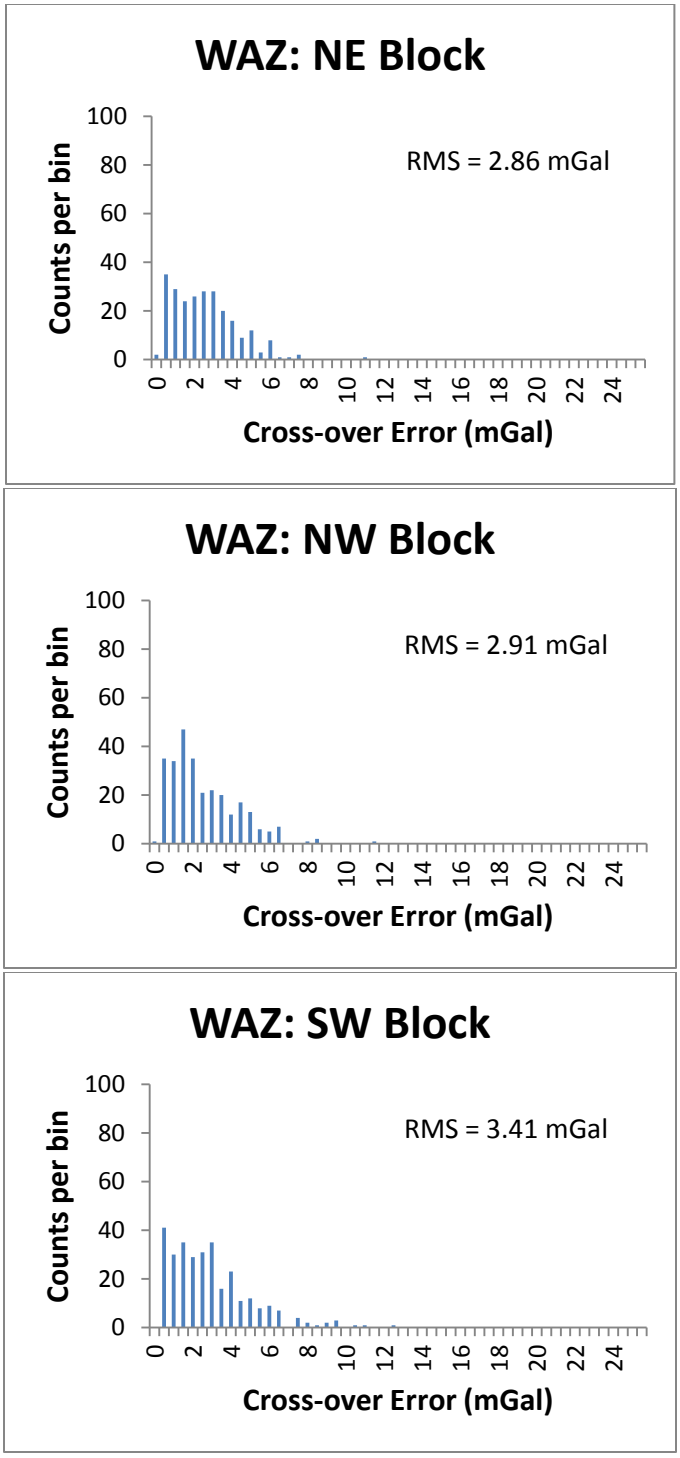

Figure 3.3b: *The histograms for the WAZ Blocks.*

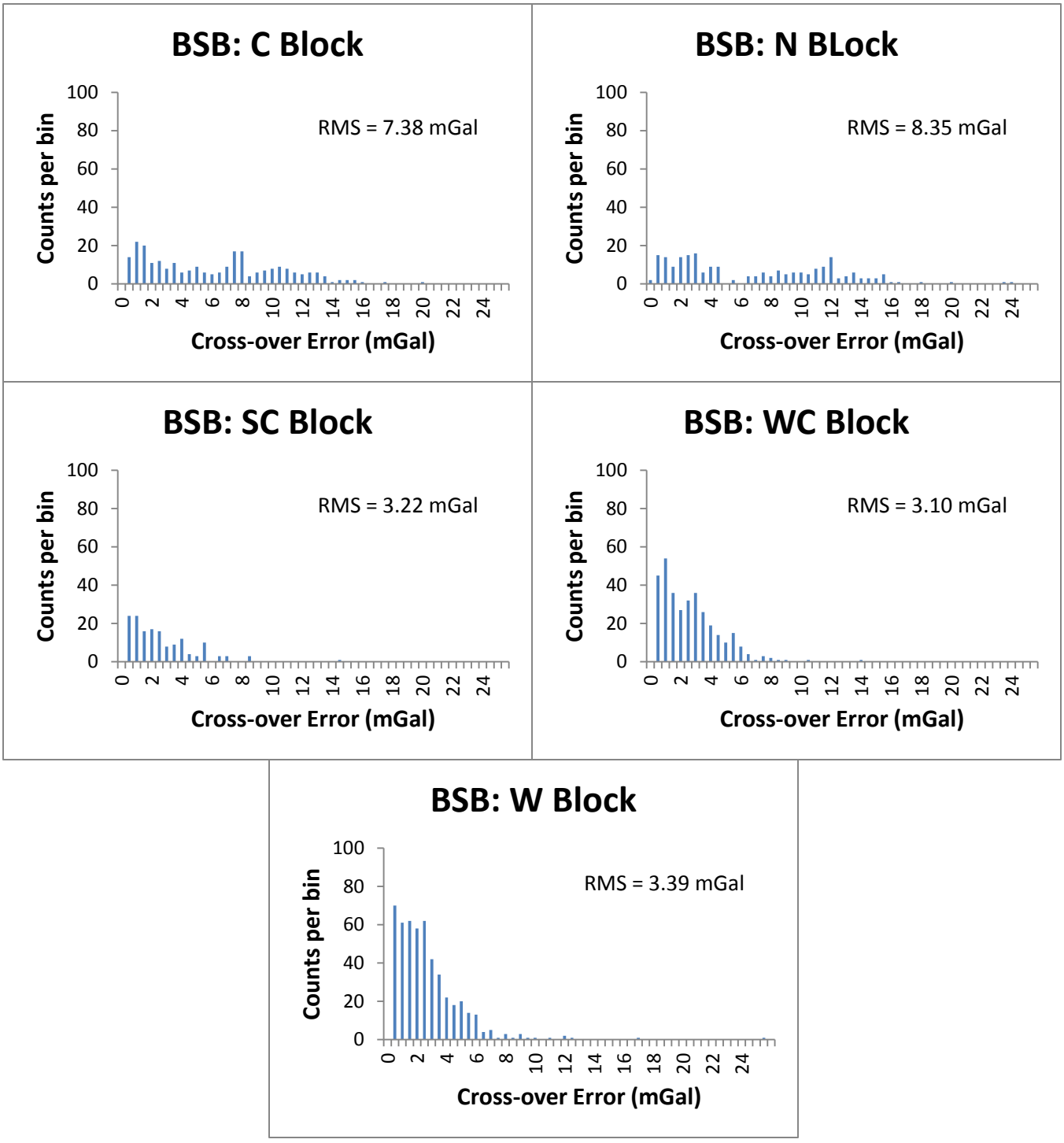

Figure 3.3c: *The histograms for the WAZ Blocks.*

3.5 RESULTS – FREE AIR GRAVITY DISTURBANCES

The result of the gravity reduction gives the free-air gravity disturbance over this part of the Siple Coast (Figure 3.4 – this figure, and all similar figures, is plotted with Generic Mapping Tools (GMT) ((Wessel and Smith, 1998) in a Polar Stereographic 71 projection). Much of the area has a negative gravity disturbance indicative of "missing" mass. The extremely low gravity point at approximately (-900E, -450N) correlates with the Bentley Subglacial Trench, while the rounded feature near (-450E, -800N) correlates with Siple Dome, a more elevated feature than Bentley Subglacial Trench. The lower right section, which consists of TKD and WAZ, shows smaller-scale linear features parallel with Bindschadler Ice Stream flow towards the Ross Ice Shelf; the thick red line indicates the grounding line of the ice shelf. In the upper right section, the topography exhibits several highly positive gravity features, along with a couple below Bentley Subglacial Trench, which could be interpreted as subglacial volcanoes, as has been done before in West Antarctica (Blankenship et al., 1993).

3.6 INTERPRETATION

The linear features parallel to the trunk of Bindschadler Ice Stream extend through its entire length. The symmetry and negative free-air gravity disturbance of these features is characteristic of sedimentary basins. The inland extent of sediments beneath the Ice Stream likely determines the extent of flow (Anandakrishnan et al., 1998; Bell et al., 1998; Blankenship et al., 2001; Studinger et al., 2001). The topography increases in relief inland, especially in the northern BSB sections; the contrast between the trunk of Bindschadler Ice Stream and the northern upstream zones also point toward the

difference between the rift floor and the rift flank. The northern BSB section abuts Marie Byrd Land, which forms part of the WARS rift flank (Figures 2.1, 2.2). The more positive free-air gravity highs suggest thicker crust, while the more negative suggest thinner crust. The most negative disturbance is over BST, which is located in the middle of the rift zone (Winberry and Anandakrishnan, 2004).

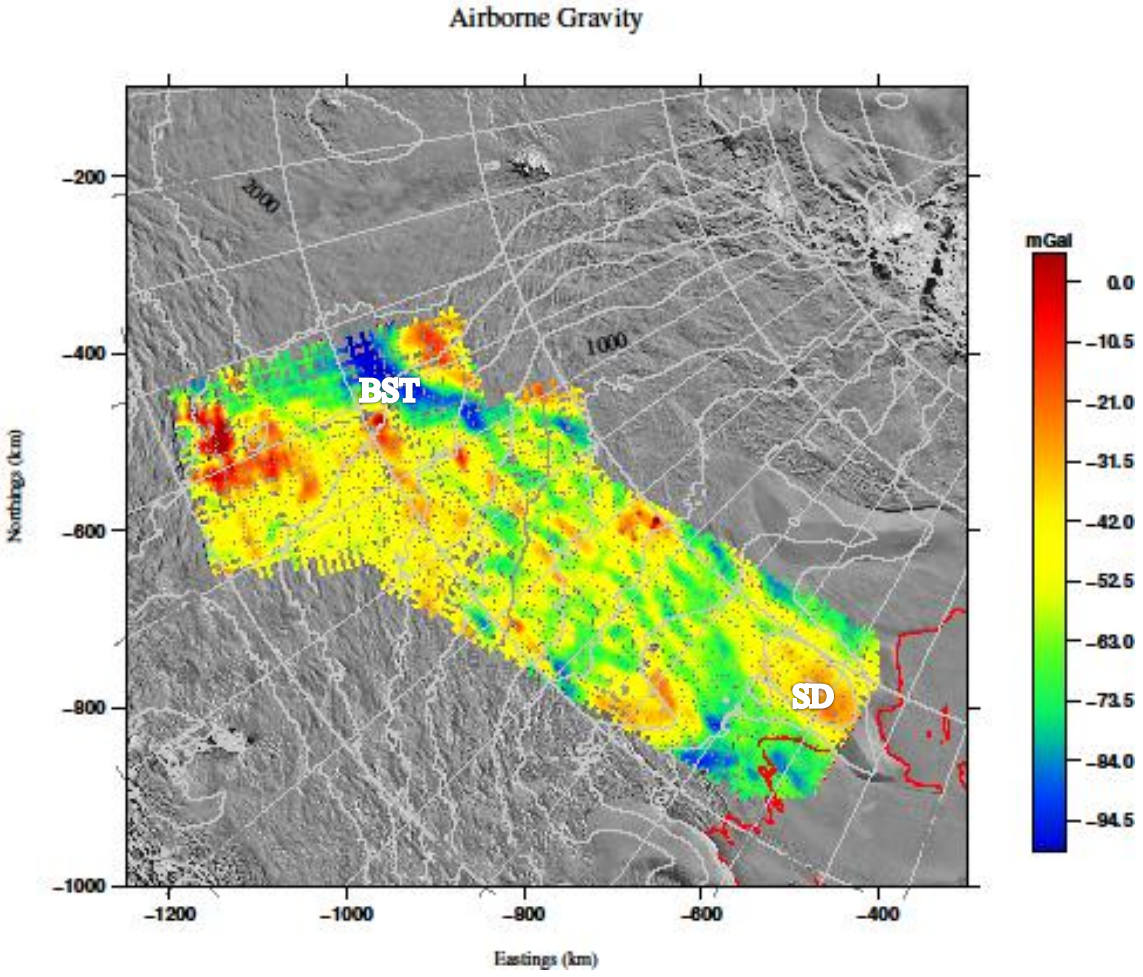

Figure 3.4: *The reduced gravity, showing the free-air gravity disturbances. BST = Bentley Subglacial Trench; SD = Siple Dome.*

Chapter 4

Airborne and Satellite Gravity

4.1 THEORY OF GOCE

While airborne gravity is more detailed over a greater area than ground based surveys, satellite gravity surveys cover a larger area – the surface of the Earth – and can do so to a high degree of accuracy. Given that gravitational attraction decreases at a rate inversely proportional to the square of the distance, a balance needs to be kept between the height of the gravity satellite and its ability to orbit. The Challenging Mini-Satellite Payload (CHAMP) was launched in 2000 and orbited at 400 km above the Earth; the Gravity Recovery and Climate Experiment (GRACE), which consisted of two satellites flying 200 km apart, was launched in 2002 and orbited at 400 km also; and the most recent, the Gravity Field and Steady-State Ocean Circulation Explorer (GOCE), was launched in 2009 and orbits at about 250 km (European Space Agency, 2010). GOCE has the highest resolution satellite and is capable of deriving a global geoid model with an accuracy of 1-2 cm, at a spatial resolution of 100 km (European Space Agency, 2010).

The gradiometer on GOCE is based on three pairs of proof masses that are located at the ends of orthogonal axes (European Space Agency, 2010). The linear and rotational motion of the proof masses is controlled by electrostatic suspension (European Space

Agency, 2010). The three axes are oriented such that one is aligned with the satellite's trajectory, one is perpendicular to the trajectory, and points toward the center of the Earth; each of these axes also has a pair of accelerometers (European Space Agency, 2010). The difference between each of pair of accelerometers, scaled by the length of the axis (50 cm) between them, is the gravity gradient; the accelerometers are 100 times more sensitive than previously flown accelerometers (European Space Agency, 2010). The entire configuration forms the electrostatic gravity gradiometer (European Space Agency, 2010). The satellite also carries a GPS receiver to use for satellite-to-satellite tracking, which is used to align the velocity vector in real time (European Space Agency, 2010). A system is also in place to account for any non-gravitational forces, such as air-drag and radiation pressure (European Space Agency, 2010).

4.2 METHODOLOGY

For this study, the GOCE gravity (Figure 4.1) was used to validate and level the long wavelength signal of the airborne gravity. Satellite gravity, due to its distance from Earth and the inverse square of the gravitational signal, is preferred for the long wavelength gravity signal, while the airborne is preferred for the short wave length signal, or the high frequency data. In order to accomplish this, one can either subtract the mean of the airborne data and then add in the mean of the satellite gravity, or one can subtract the mean of the differences between the airborne and satellite gravity. The latter method was used, with the mean of the differences for each zone shown in Table 4.1.

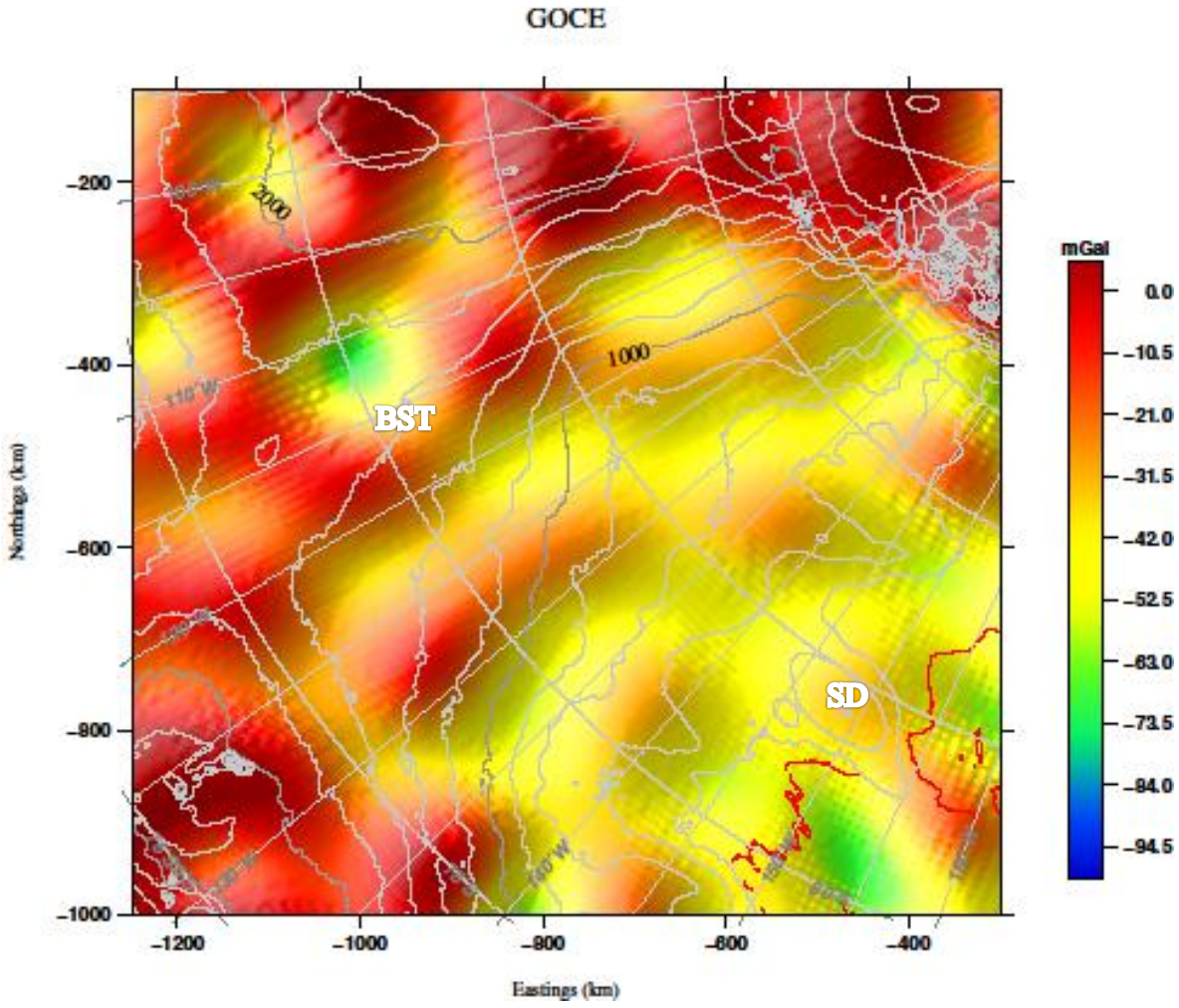

Figure 4.1: *The GOCE satellite gravity data. Note the large-scale features that are captured, while no small-scale features are seen. BST = Bentley Subglacial Trench, SD = Siple Dome.*

Table 4.1: *Mean of the differences between airborne and satellite gravity.*

Block		Mean of differences (mGal)
BSB	C	-20.48
	N	-18.87
	SC	-22.66
	WC	-21.06
	W	-12.62
TKD	C	-6.97
	NE	-1.15
	SE	-4.05
	W	-7.26
WAZ	NE	-6.79
	NW	-9.58
	SW	-14.89

4.3 RESULTS

The results of the leveling (Figure 4.2) bring to the forefront more small-scale features, especially in the trunk of Bindschadler Ice Stream. In comparison to the unleveled data (Figure 4.3), Siple Dome becomes more distinct while Bentley Subglacial Trench gravity disturbance becomes less negative. Positive gravity features also become more apparent in the upper left corner, along with a larger feature just above Bentley Subglacial Trench. When compared to just the GOCE gravity (Figure 4.1), it can be seen that the satellite gravity did not capture small-scale features like the linear features along the trunk of Bindschadler Ice Stream or even the extension of the Bentley Subglacial Trench towards the Ross Ice Shelf. The GOCE gravity also reflects the gradual negative gravity trend from left to right as well. The airborne gravity locates the high frequency,

short wavelength features better, while the satellite gravity enhances the low frequency, long wavelength features.

4.4 INTERPRETATION

The removal of terrain features from the gravity disturbances in the Bouguer map (Figure 5.3) shows that Siple Dome is mainly a topographic feature, as it is not distinct in Bouguer disturbance map. The Bouguer disturbances become regionally more negative towards the northern, upstream end, especially near the intersection of WAZ and BSB, implying thicker crust, which we propose for the rift flank. The topographic high south of the BST (Figure 4.3) becomes a highly negative disturbance in the Bouguer analysis, indicating isostatic compensation or possibly underplating; in contrast, the northern half, for which the free-air gravity was not so positive indicating that more of the free-air gravity disturbance was due to the crust, rather than topographic features. Being farther from the center of the rift, unlike the area near BST, the crust would be less rifted and thicker. The positive Bouguer disturbances could also be indicative of volcanic material and subglacial volcanism has played a part during the rifting process (Paulsen and Wilson, 2010).

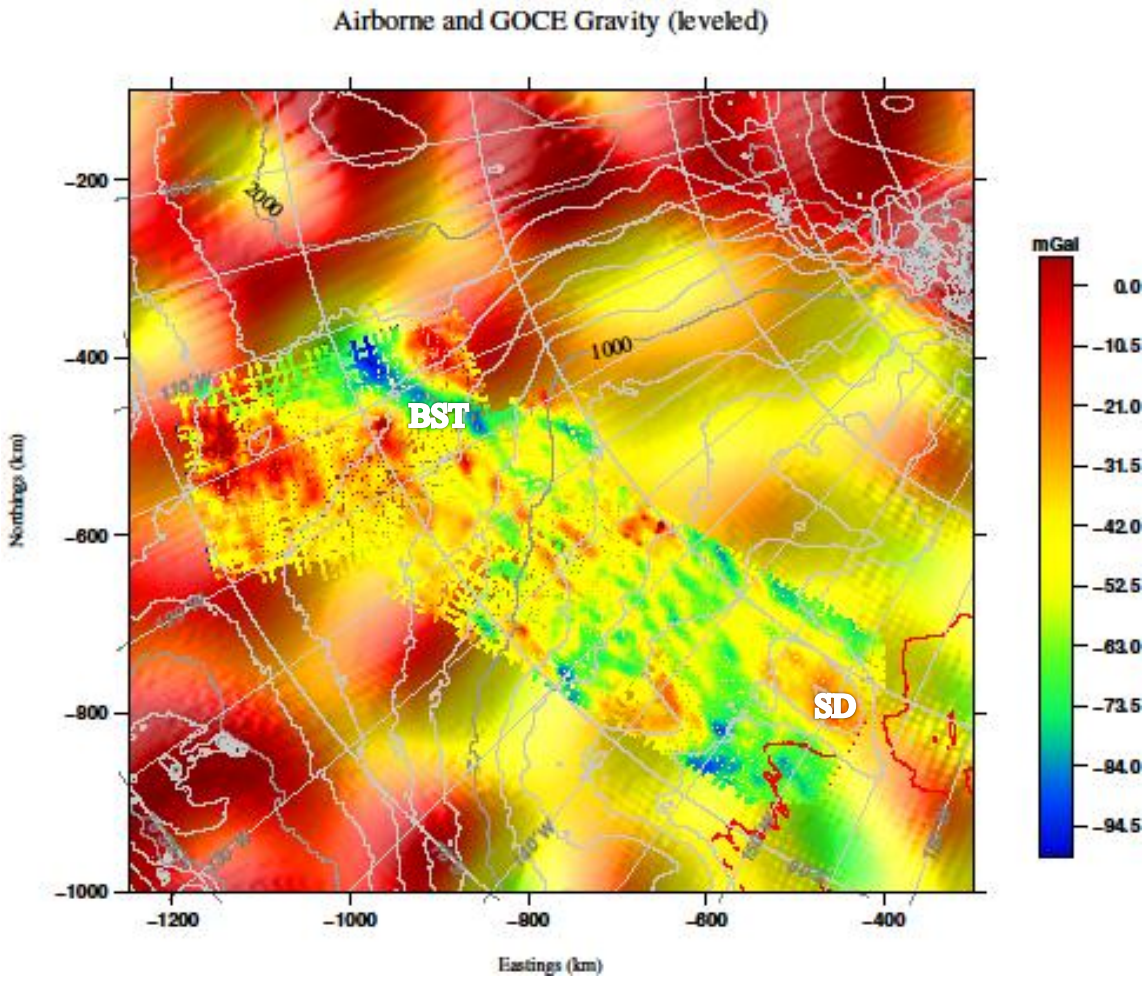

Figure 4.2: *The airborne gravity data leveled by removal of its mean values and replacing them with the GOCE satellite mean values. The GOCE gravity values are overlaid by the airborne gravity.*

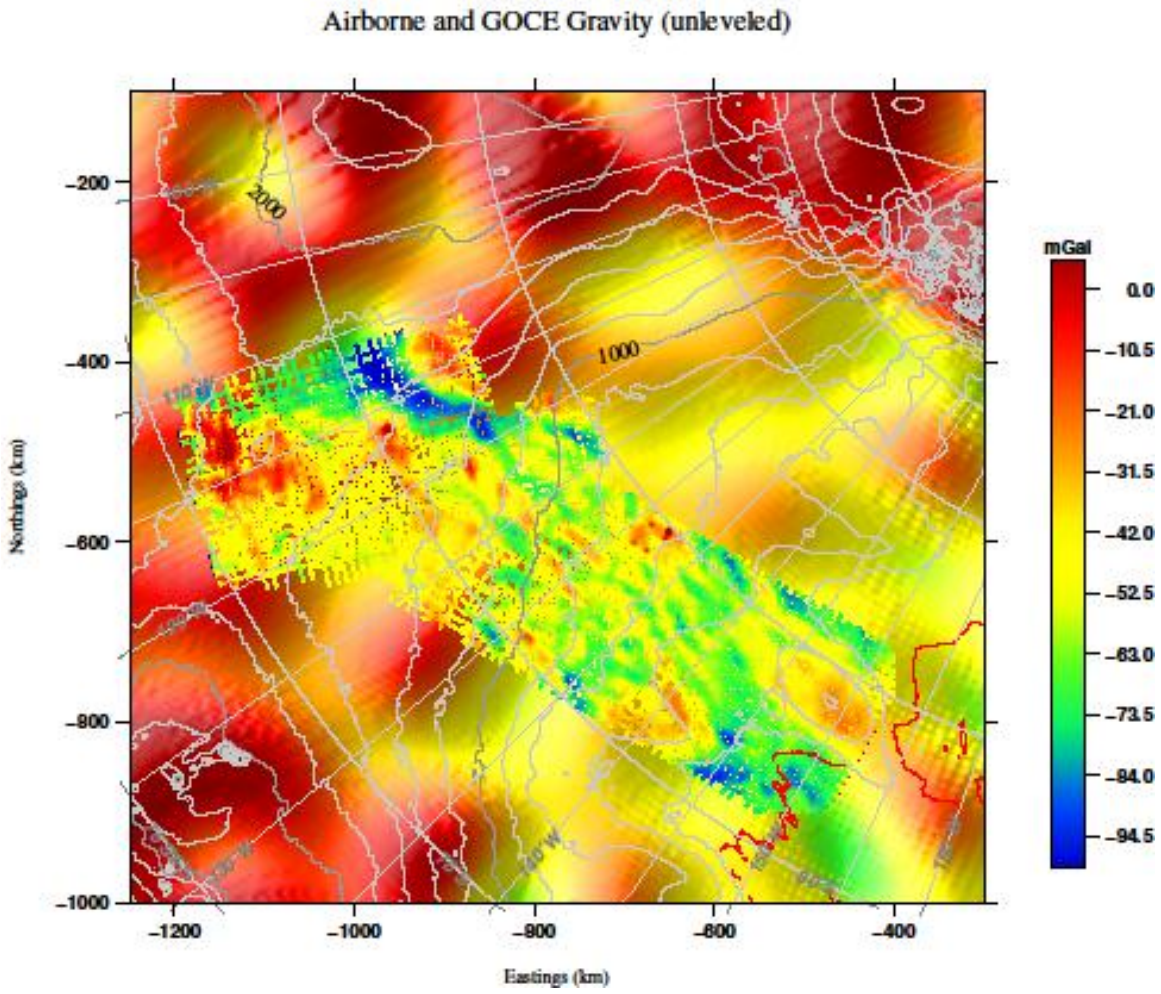

Figure 4.3: *The GOCE gravity values are overlaid by the unleveled airborne gravity for comparison with Figure 4.2.*

Chapter 5

Bouguer Disturbance

5.1 THEORY

The removal of instrument, Eötvös, latitude, and acceleration corrections has given the free-air disturbance over the Siple Coast. The further removal of the effects of topography gives the Bouguer disturbance; the Bouguer disturbance is the end product of all gravity corrections and should correlate with the lateral density variations within the crust and Moho topography. The Bouguer correction is traditionally applied in three steps: the Bouguer slab correction which estimates the topography as a slab with infinite lateral extent, constant density, and thickness equal to the elevation of the measurement point with respect to mean sea level (Bullard A); the curvature correction, which replaces the slab with a spherical cap that remains the same thickness to 166.735 km (Bullard B); and, the terrain correction which accounts for the surrounding topography both above and below the point of calculation (Bullard C) (Bullard, 1936). The terrain correction is positive for on-shore points, and either positive or negative for off-shore points (Fullea et al., 2008). Terrain calculations were traditionally carried using Hammer's (1939) method, which divides the area surrounding a point into cylindrical sectors and compares the measurement point elevations with the cylinder elevation; improvements to the

methodology have come with increased computing power, digital elevation models (DEMs), and numerical algorithms, such as Fast Fourier Transform (Banerjee, 1998; Forsberg, 1985).

In this analysis, FA2BOUG, a FORTRAN 90 program developed by Fullea et al. (2008), was used to compute the 2D Bouguer disturbance. As with the free-air disturbance, this calculation is termed a 'disturbance' rather than an 'anomaly' because the goal is to remove large-scale gravity effects that mask the local anomalies of interest (Hackney and Featherstone, 2001). FA2BOUG works on grid-based computations, performing the Bullard A, B, and C corrections based on several zones which depend on a distance R from the calculation point (Fullea et al., 2008). The calculation is also influenced by being on- or off-shore, where on-shore ($h > 0$) and off-shore ($h < 0$) is defined by h, the elevation of the calculation point. In the initial calculation, ice above sea level is not accounted for, but it is separately treated as a simple Bouguer slab and removed later.

The input parameters for the program can be modified, but certain parameters, like density, remain constant. The input parameters are:

1. whether a detailed on-shore topography is used (one was not used in these calculations),
2. grid step for the intermediate ($\Delta x_i = 2\ km$) and distant ($\Delta x_d = 4\ km$) calculation zones,
3. the grid step for the output Bouguer disturbance grid ($\Delta x_{Bg} = 3.70591\ km$),

4. reduction density for the crust ($\rho = 2670\ kg/m^3$),
5. reduction density for the water, but these calculations used ice instead of water ($\rho = 910\ kg/m^3$),
6. the expected limits of the intermediate and distant zones as the number of grid cells, $N\ x\ M$,
7. the limits of the intermediate ($R_i = 20\ km$) and distant ($R_d = 167\ km$) zones,
8. whether or not the calculation includes both on-shore and off-shore points (all input grids were treated as having both, since off-shore is defined as $h < 0$, and
9. whether the input gravity data is a simple Bouguer slab or free-air (the input data was in the form of free-air disturbances).

The intermediate and distant zones (R_i, R_d) are defined to be 20 and 167 km, respectively by the Fullea et al. based on both testing and theory. The intermediate zone, R_i, is set to 20 km to provide an accuracy of 0.1 mGal, and the distant zone, R_d, at 167 km coincides with the outer limit of the Hayford-Bowie system of 167.734 km (1.5^o) which minimizes the difference between the effects of the infinite horizontal Bouguer slab and the spherical cap (Hayford and Bowie, 1912; LaFehr, 1991b).

5.2 METHODOLOGY

To prepare the input gravity data, the leveled gravity data, in the form of Cartesian longitude and latitude and gravity disturbance (mGal) was turned into a grid with GMT codes, using a GMT built-in spline interpolation. The interpolated grid has a

cell size of 2 km, which is equal to the grid step of the intermediate zone, x_i. The outer limits of the gridded region were set to 167 km farther on all four sides to account for how FA2BOUG runs, that is, FA2BOUG outputs a Bouguer anomaly grid that is decreased R_d on all sides from the original input data; the 167 km trimming occurs due to the Bullard B correction in the program (Fullea et al., 2008).

The input parameters for each area only varied the number of points in each grid, *N x M* (Table 5.1). The grid steps for the intermediate and distant zones and the output Bouguer grid step were kept as in the published FA2BOUG program (Fullea et al., 2008), which produces an output Bouguer map that has a grid step of Δx_{Bg} = 4 km. The program also has an internal coordinate system, which is dereferenced from original Cartesian coordinates, simply labeling the northwest corner of the input grid as *(0,0)*, and moves from west to east successively and ends in the southeast corner (Fullea et al., 2008).

Table 5.1: *The blocks used in the Bouguer calculation, the number of grid cells, and the elevation range of the aircraft.*

Block		N	M	Elevation Range (m)
BSB1	C, N, WC	300	400	308
BSB2	SC	244	400	245
BSB3	W	296	400	241
TKD	C, NE, SE, W	298	400	354
WAZ1	NE	274	200	256
WAZ2	NW, SW	297	600	273

In order to maximize the study area for each Bouguer calculation, and also to separate zones flown at different elevations, sub-sections were created (Table 5.1; Figure

5.1). These were a total of six sections for which Bouguer disturbances were calculated. As with the airborne and satellite gravity, all maps were plotted with GMT (Wessel and Smith, 1998). The errors in BSB blocks C and N that were discussed in Chapter Four show up in the Bouguer results due to unleveled lines skewing the analysis.

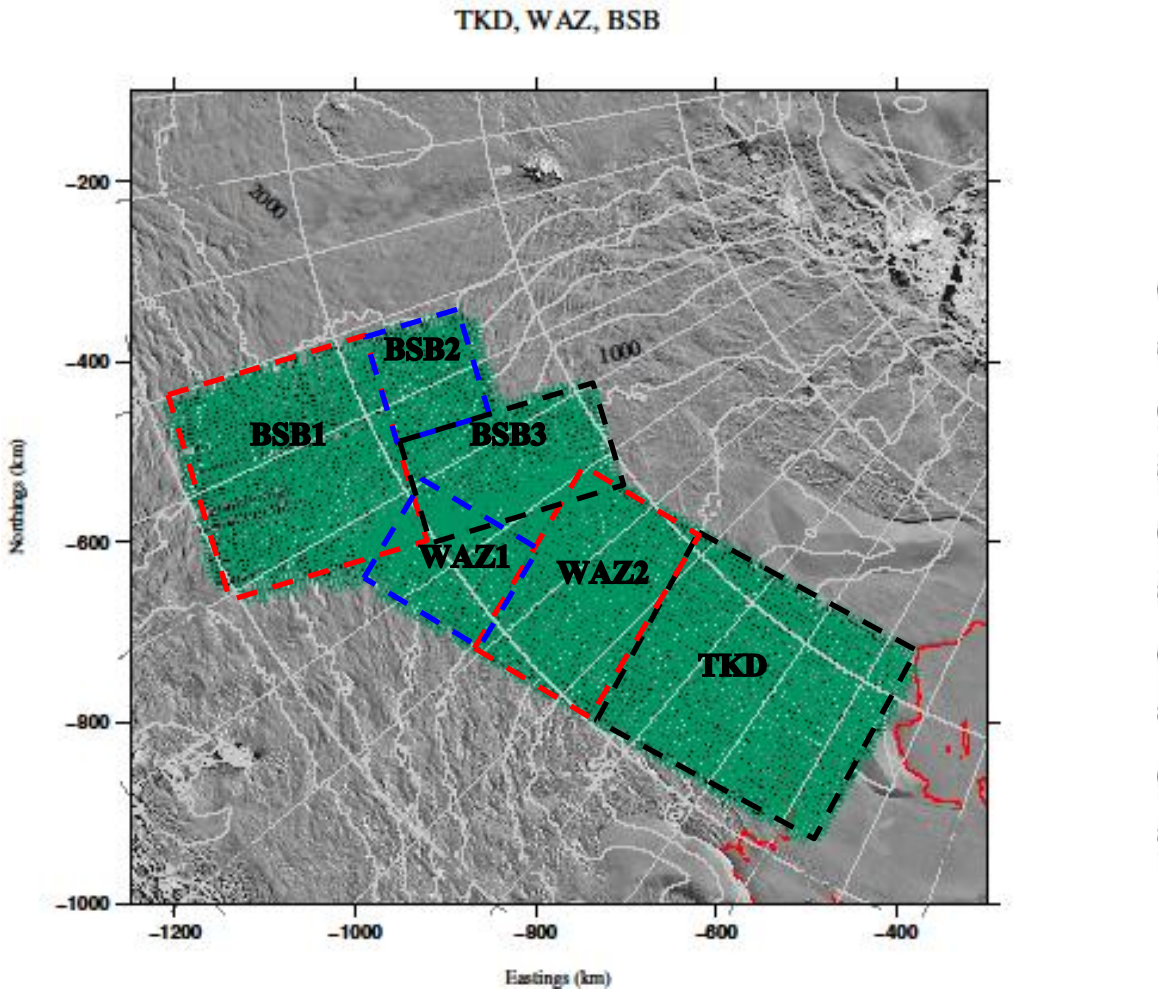

Figure 5.1: *The sections used for Bouguer calculations in FA2BOUG.*

In the first set of figures, the Bouguer disturbance is given without a correction for the gravity disturbance caused by the overlying ice. The Bouguer disturbance is then given with the ice correction above sea level. The ice is treated as a simple Bouguer slab, which is computed with:

$$g_B = 2\pi\rho GH$$

where ρ = 910 kg/m^3 (density of ice), G is the gravitational constant (6.67 x 10^{-11} m^3/s^2/kg), and H is, in this case, the surface elevation. This correction was applied to the gridded Bouguer disturbances.

5.3 RESULTS

Keeping in mind that each section was input into the FA2BOUG program from the NE to the SW corner (Fullea et al., 2008) and that the coordinates are relative to the program, Figure 5.2 represents the Bouguer disturbance without a correction for the ice thickness above sea level in the survey area. While the minimum and maximum Bouguer disturbances vary greatly – both positively and negatively -- the mean value for each block is mostly positive (Table 5.2).

With a correction for ice thickness, generally, the Bouguer disturbances show a trend of becoming more negative from the upstream end (BSB) to the downstream end (TKD) (Figure 5.3). There is an accepted relationship between positive Bouguer anomalies relating to thin crust and negative Bouguer anomalies relating to thick crust (Lawrence et al., 2006a; Jordan et al., 2009; Fullea et al., 2008). There are also several, smaller, well contained positive Bouguer disturbances ranging from 0-20 mGal, all which

also correlate with topographic contours. The ~ -20 mGal disturbance throughout TKD and BSB corresponds with sedimentary basins proposed based on the previous analysis of this data and magnetics data (Bell et al., 2006).

5.4 INTERPRETATION

As the topographic influences have been removed in the Bouguer disturbance used in the power spectrum analysis, the 3.2 km density contrast (Figure 6.4) is due to an anomaly near the ice-bed interface, which could be the proposed sediment basin. The density of crust used in this study is 2670 kg/m^3, while sediment density, on average, is closer to 2150 kg/m^3. The location of sedimentary basin(s) in this region is supported by both previous analysis (Bell et al., 2006) and seismic studies of the upstream area (Winberry and Anandarishnan, 2004; Peters et al, 2006). A sedimentary basin, in combination with a till-water system, will aid ice stream flow. As ice streams are the most dynamic components of the ice sheet, knowing their bed parameters leads to better understanding of their controls and extents. This knowledge is especially important since sediments control the inland extent of ice streams.

Identifying the rift floor and flank bring better understanding of the nature of the rift and Marie Byrd Land's compensation. The thicker crust of Bindschadler Ice Stream (27.5 km) and the thinner crust of the rift shoulder (25 km) are possibly indicative of: 1) thermal compensation of the rift shoulder, 2) higher density crust in the rift floor, and/or 3) underplating of the rift floor by more magnetic material. Extended continental crust

supported by low density mantle would be Pratt isostatic compensation, while deep crustal roots are Airy isostatic compensation.

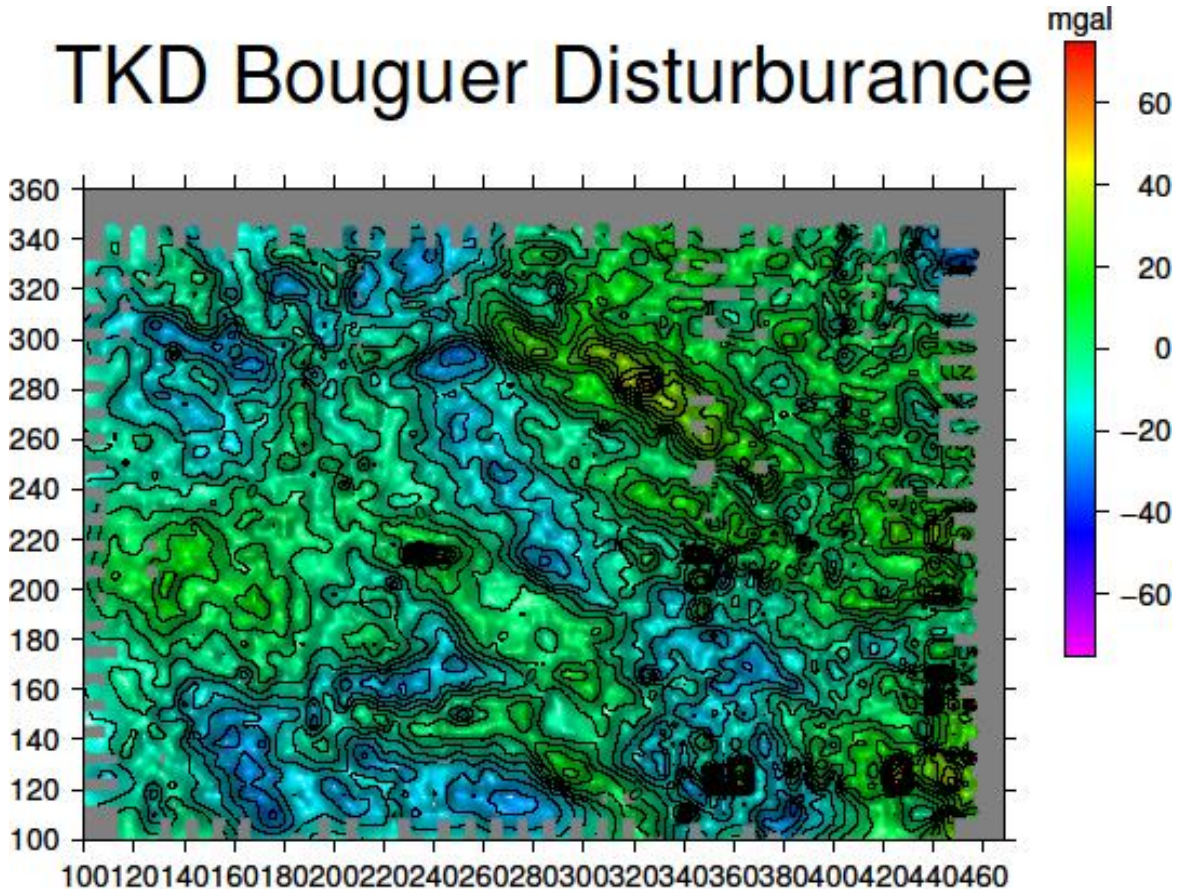

Figure 5.2a: *The Bouguer disturbances without correction for ice above sea level.*

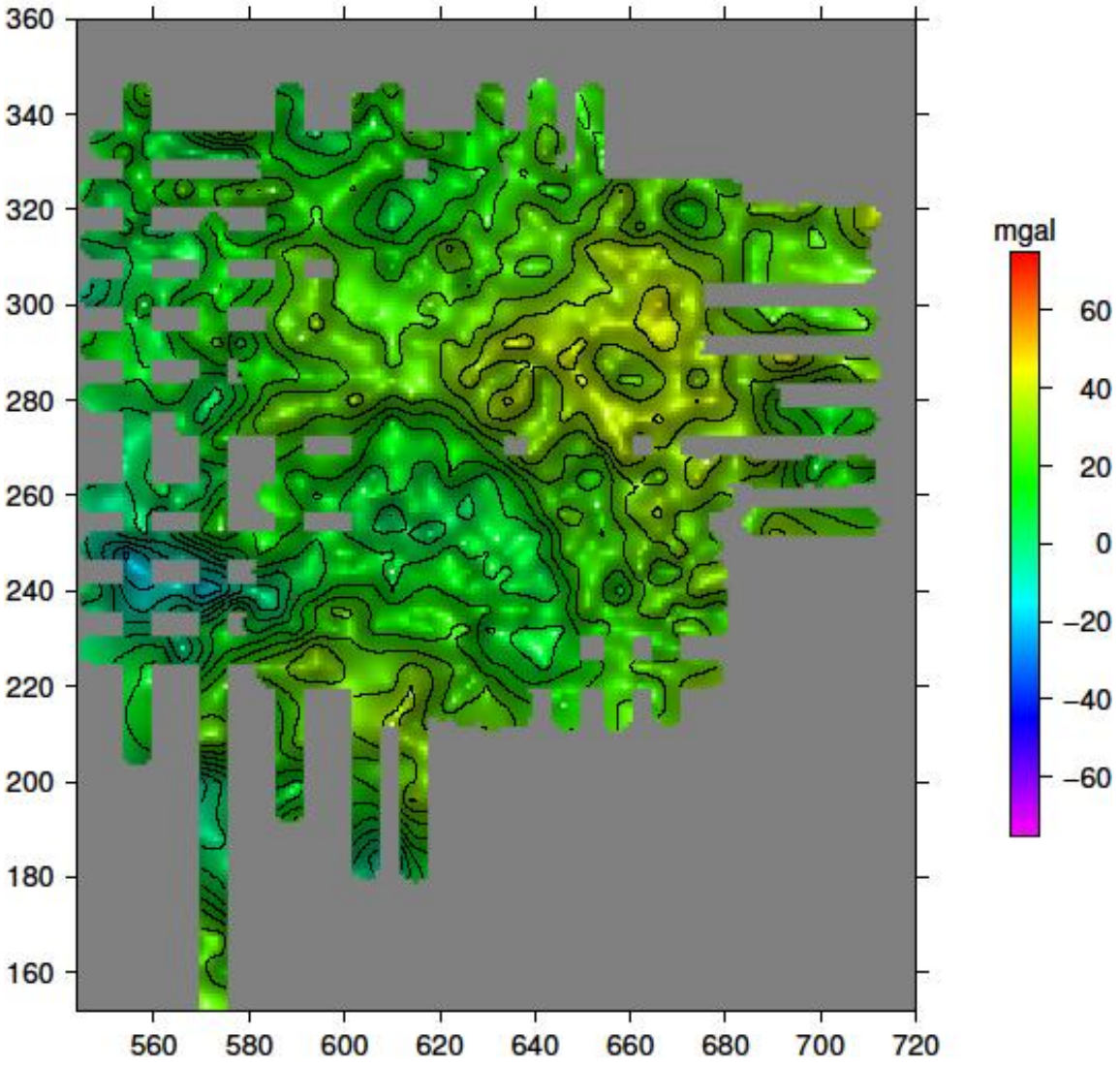

Figure 5.2b: *The Bouguer disturbances without correction for ice above sea level.*

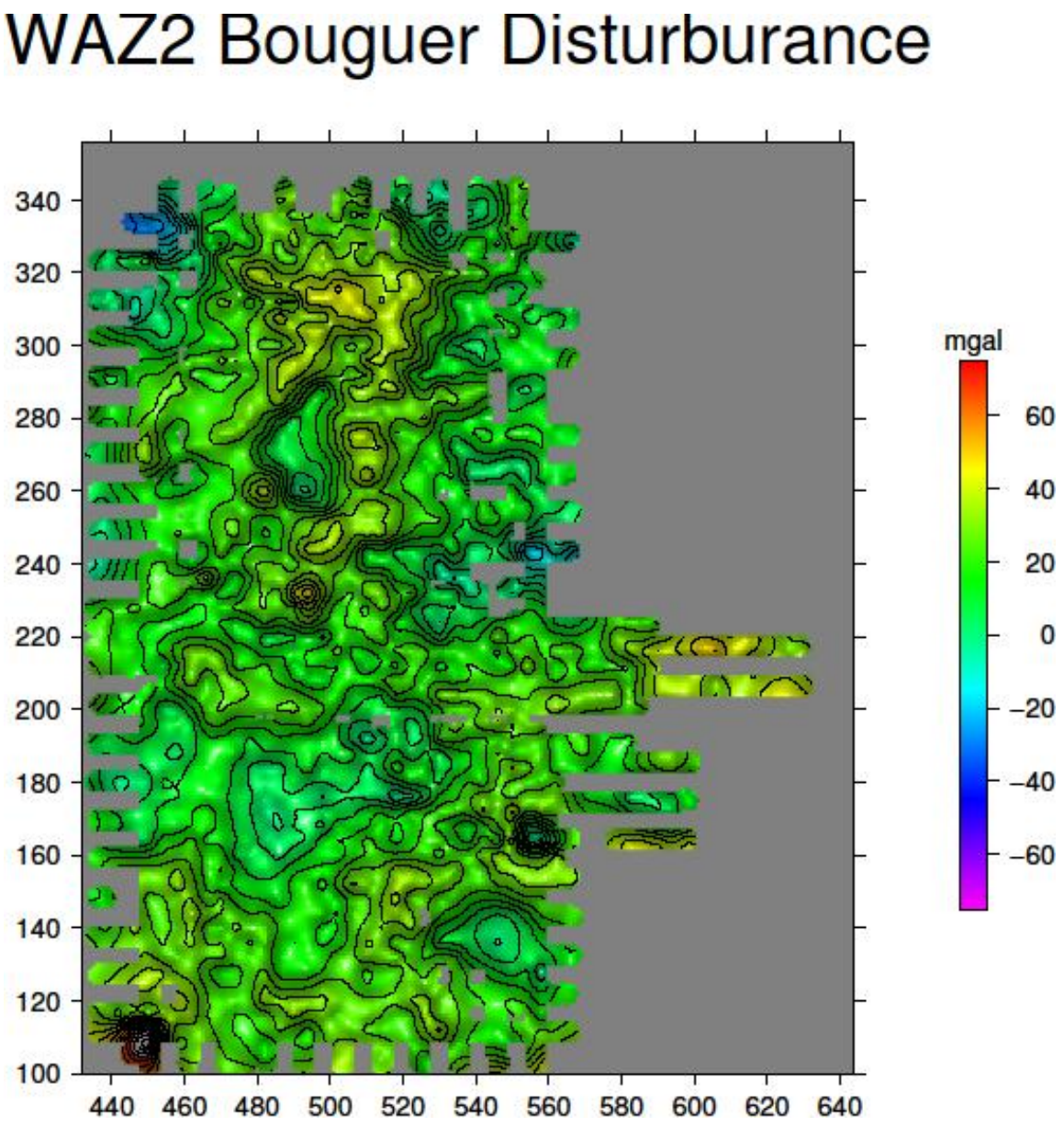

Figure 5.2c: *The Bouguer disturbances without correction for ice above sea level.*

BSB3 Bouguer Disturbance

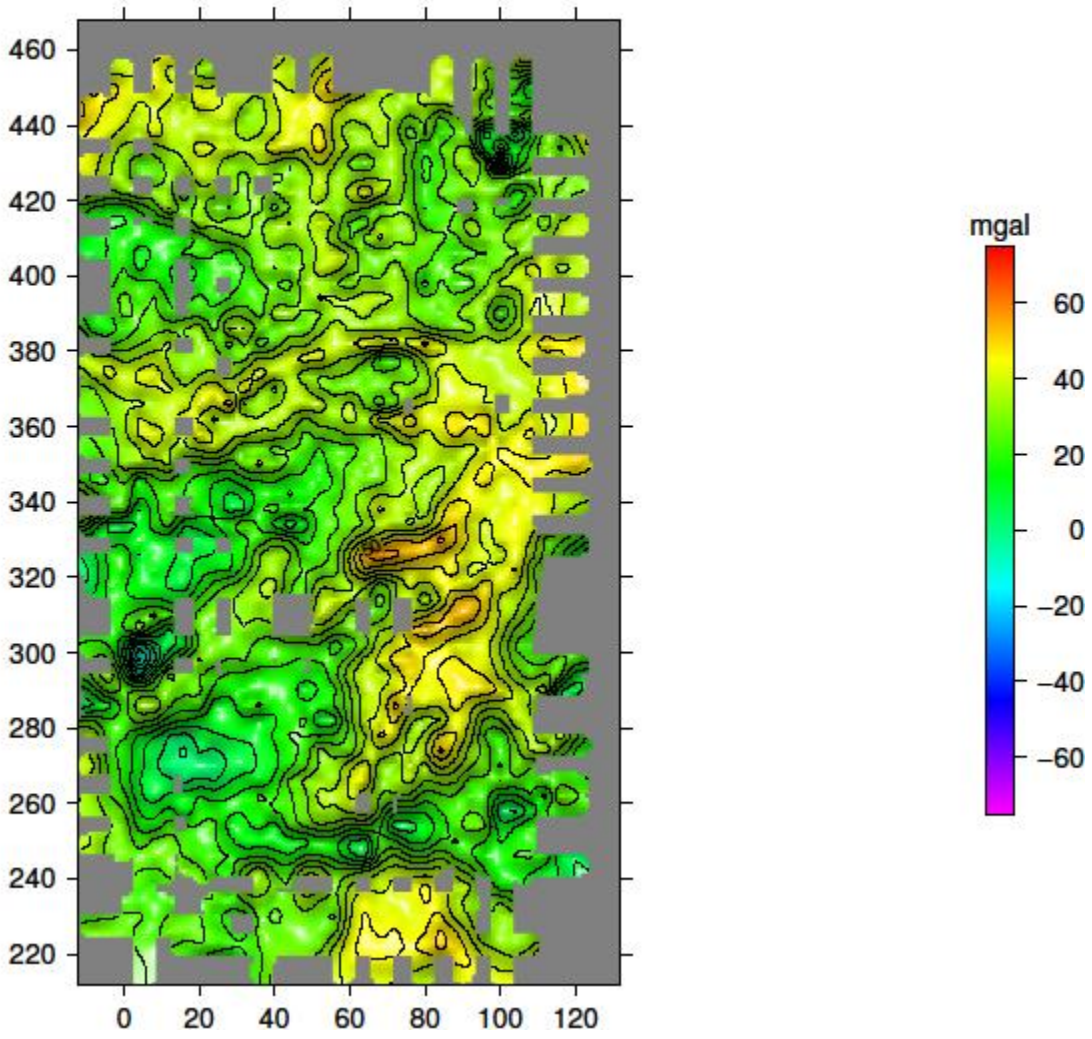

Figure 5.2d: *The Bouguer disturbances without correction for ice above sea level.*

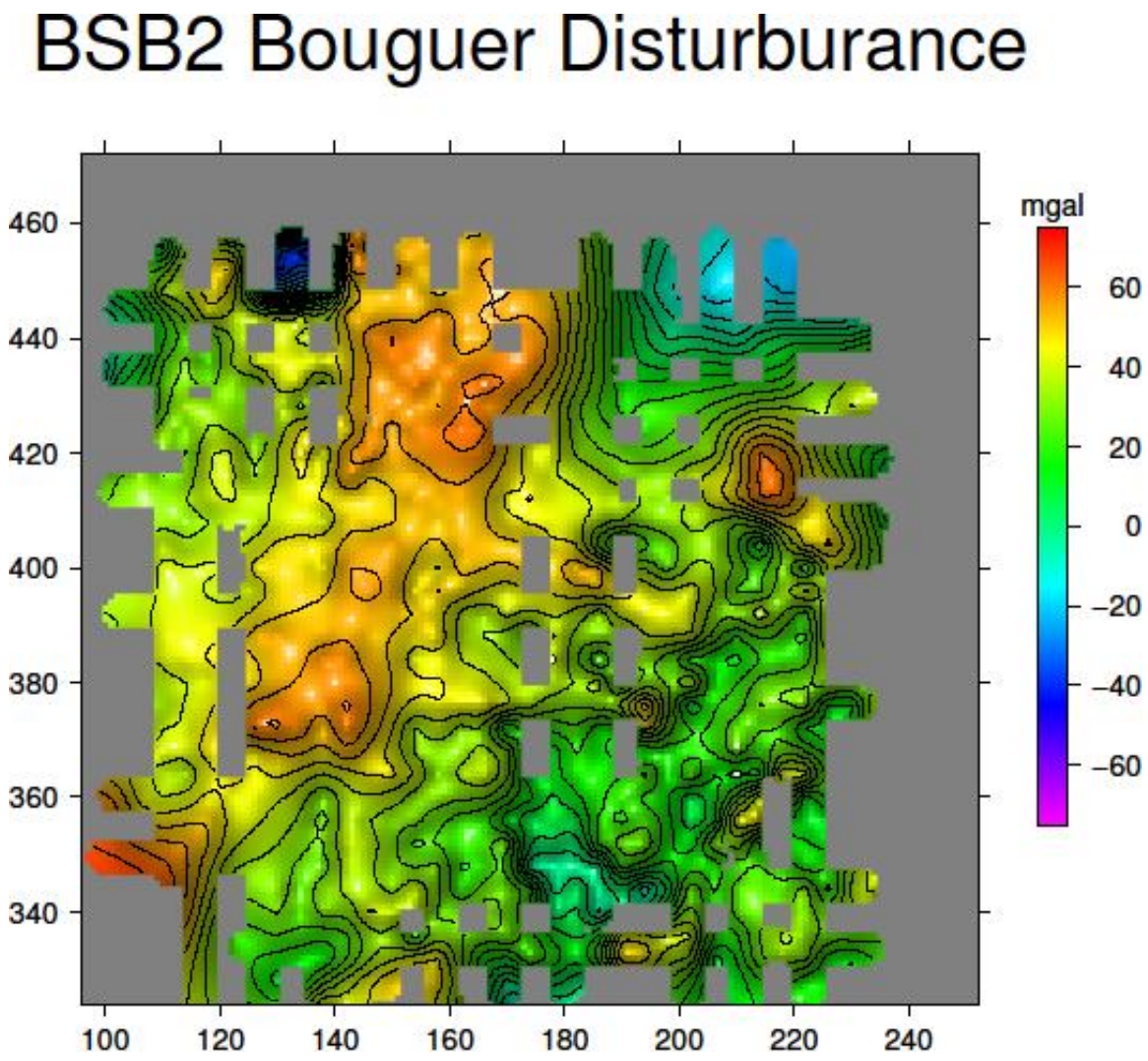

Figure 5.2e: *The Bouguer disturbances without correction for ice above sea level.*

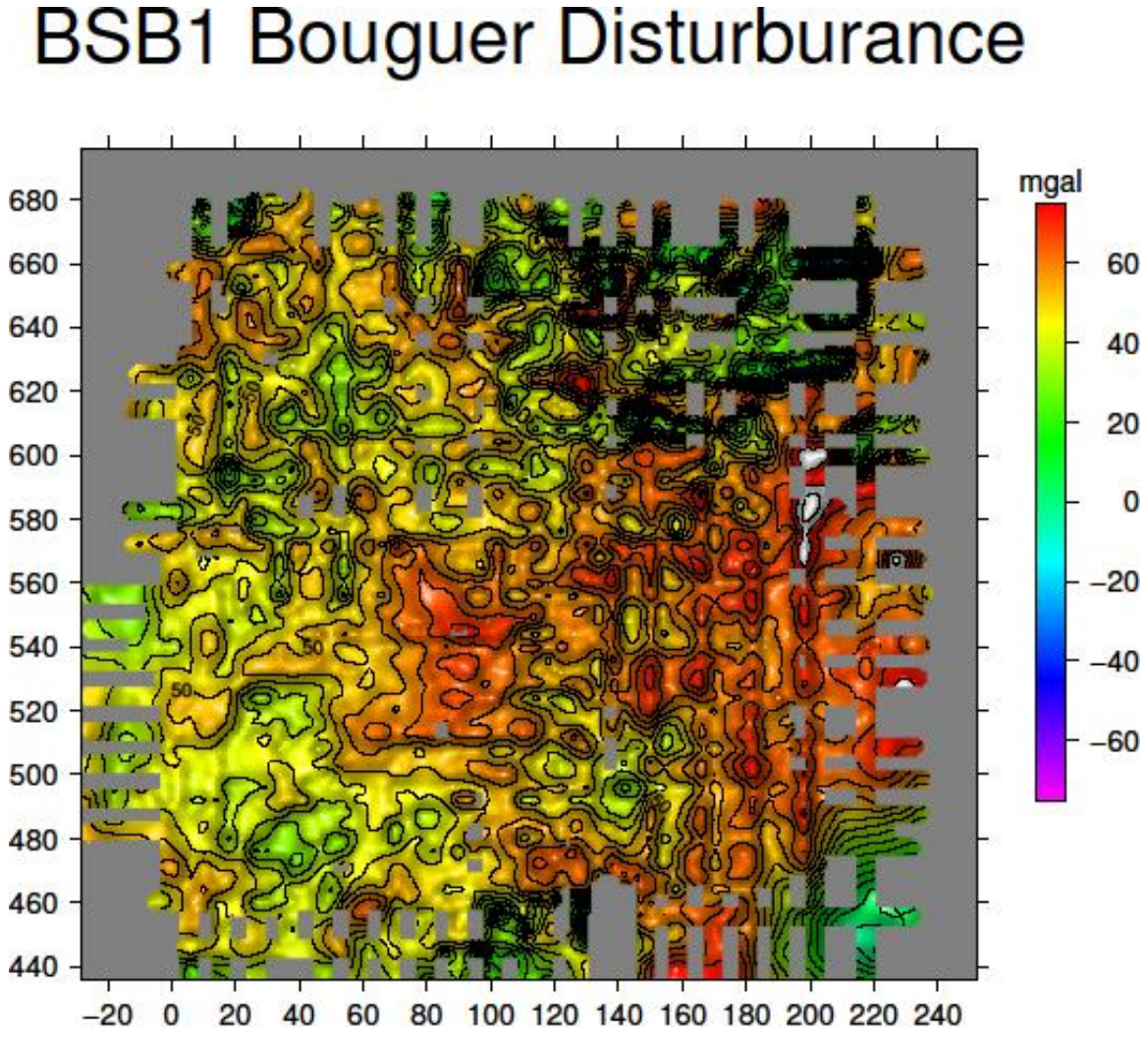

Figure 5.2f: *The Bouguer disturbances without correction for ice above sea level. Note that the multiple seasons for BSB C and N affect this grid with the errors that are due to lines that are not level to each other.*

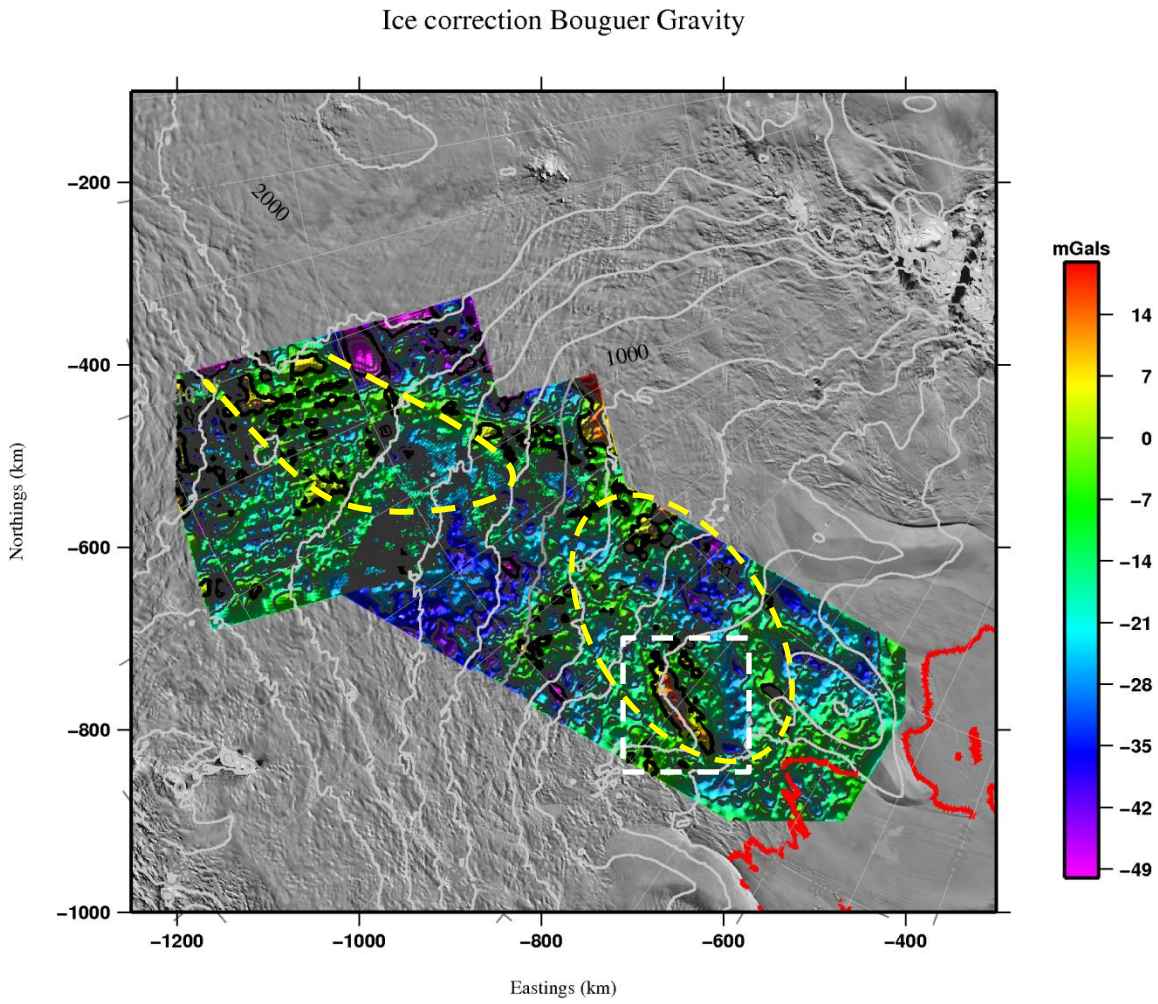

Figure 5.3: *The Bouguer disturbances with a correction for ice above sea level. White box outlines the major positive disturbances referenced in the text; yellow circles show the approximate borders of the sedimentary basins from Bell et al. (2006).*

Chapter 6

Spectral Analysis

6.1 THEORY

The combination of independent, subsurface prisms creates the observed potential field of a region (Spector and Grant, 1970), in this study, the Bouguer gravity distribution. The depth of these prisms is the dominate factor in the power spectrum, i.e. the square of the Fourier amplitude spectrum, if the thickness of the prism is very small in comparison to the mean depth (Spector and Grant, 1970). As the size of the prism only influences the decay rate of the spectrum, the size is usually ignored in order to calculate the maximum depth estimate based entirely on the observed potential field data and without separation of the data into regional and residual components (Fairhead and Okereke, 1988). The power spectrum, then, is composed of an averaging of the influencing densities, e.g. the different layers of the earth below the surface, and sections of the power spectrum can be identified as density boundaries.

Discrete density boundaries can be obtained by computing the power spectrum of either free-air or Bouguer gravity anomalies (Spector and Grant, 1970; Karner and Watts, 1983; Fairhead and Okereke, 1988). A power spectrum analysis works on gravity data without the use of *a priori* data so it is well suited for this area, which has not had a

comprehensive seismic study (Peters et al., 2001) and where magnetics studies have only been used to identify sedimentary basins (Bell et al., 2006). Breaks in the power spectrum indicate that there has been a change in the crustal density at depth, and the one-half of the slope between breaks is the depth in the lithosphere to that density contrast (Spector and Grant, 1970; Karner and Watts, 1983; Fairhead and Okereke, 1988). The area also needs to be relatively homogenous or else the breaks in the spectrum cannot be easily identified (Spector and Grant, 1970).

6.2 METHODOLOGY

The power spectrum was computed over an area 30 km wide and 600 km long, beginning at the Ross Ice Shelf end of TKD and extending along latitude lines separated by 5 km until the in-land most end of BSB, excluding the BSB1 block, which has spurious data. The spectrum itself was computed with GMT's 1D spectrum routine on the Bouguer gravity disturbance data. The spectrum is plotted up with the wavenumber, k = *1/wavelength,* against the log (base 10) of the spectrum (Fairhead and Okereke, 1988). Then, portions of the spectrum were to fit to straight line segments that occur between breaks in the power. The resulting depth to the density boundary is calculated with:

$$d = \frac{m}{2}$$

where d is the depth to the density contrast and m is the slope of the line segment (Fairhead and Okereke, 1988). The endpoints of the line segments were chosen by eye,

and then Excel's built-in linear regression line was used to find the best fit line and its slope.

6.3 RESULTS

The power spectrum is given with its error bars in Figures 6.1 and 6.3, while the power spectrum with its density boundary line segments is in Figures 6.2 and 6.4. The error bars on spectrums (Figures 6.1, 6.4) are one standard deviation. The two sets of figures either include or exclude the Bentley Subglacial Trench (BST), with its thin crust of only 21 km (Winberry and Anandakrishnan, 2004). There are three spectrum breaks, the slope of which indicates crustal density boundaries, including BST, at 20.6 ± 1.1 km, 11.5 ± 1.2 km, and 7.0 ± 1.3 km. These estimates are the depths to the Moho, a mid-crustal boundary, and a possible near-surface density anomaly. While the depth to the mid-crustal boundary is about the same as in in Diehl (2008) at 12.7 ± 1.9 km, the Moho boundary is much higher than Diehl's 29.8 ± 2.9 km. However, once the BST is removed from the crustal density boundary calculations, the boundaries fall at 27.5 ± 1.1 km, 14.9 ± 1.1 km, and 7.6 ± 1.1 km, which puts the Moho boundary within the same range. In the second power spectrum (Figure 6.4), there is also a density boundary at 3.2 ± 0.8 km, which correlates with a density anomaly at the ice-bed interface. In this study, the area for which the density contrasts were calculated was also smaller, 600 x 30 km^2 versus 200 x 200 km^2.

The crustal density estimates do not extend past 4 km, as that is the resolution of the Bouguer data on which the spectrum is based, and aliasing occurs past that point ($k = 0.25\ km^{-1}$). The noise floor after that point is much more apparent in the spectrum with BST (Figure 6.2) than in the spectrum without (Figure 6.4). The beginning of noise after

4 km is more obvious in the first spectrum (Figure 6.2) because BST is much bigger in Bouguer data than the actual topographic extent due to poor topographic definition in the data used for the Bouguer calculations; the topography for the Bouguer came from ice penetrating radar data gathered with the gravity data. The highly anomalous crustal thickness (21 km; Winberry and Anandakrishnan, 2004) also causes large density disruptions. There were two more profiles used in the power spectrum with BST than without (7 profiles versus 5 profiles), which would increase the amount of noise, making it more obvious as well. However, in seeing how well defined the data is for the 7.0 km line segment (Figure 6.2), the high frequency content is much more interpretable, recovering frequency signals at less than 10 km, which is consistent with the data processing which the gravity has undergone.

The increasing crustal depths in Figure 6.4 reflect the more northern side of the survey area, which extends onto the WARS rift floor abutting the Marie Byrd Land dome and the northern rift flank there (Figure 2.1). Seismic surveys in the area have only extended towards the southern flank of Marie Byrd Land placing the crustal thickness at 25 km and attributing it to possible support from low density mantle (Winberry and Anandakrishnan, 2004). The varying crustal thickness (20.6 km, 27.5 km and the 25 km from seismic studies (Winberry and Anandakrishnan, 2004)) demonstrate the need for better understanding of the crustal structure and isostatic compensation.

These crustal density boundaries, combined with the Bouguer disturbance distribution can in future work be combined to define the parameters of an inversion scheme. The results of inverting the data would give the size and depth of the sedimentary basins in the region. Sedimentary basins, as discussed in Chapter Two, are

essential for influencing the base of the overlying ice stream by providing lubrication and a less-resistive bed over which to flow than just bedrock.

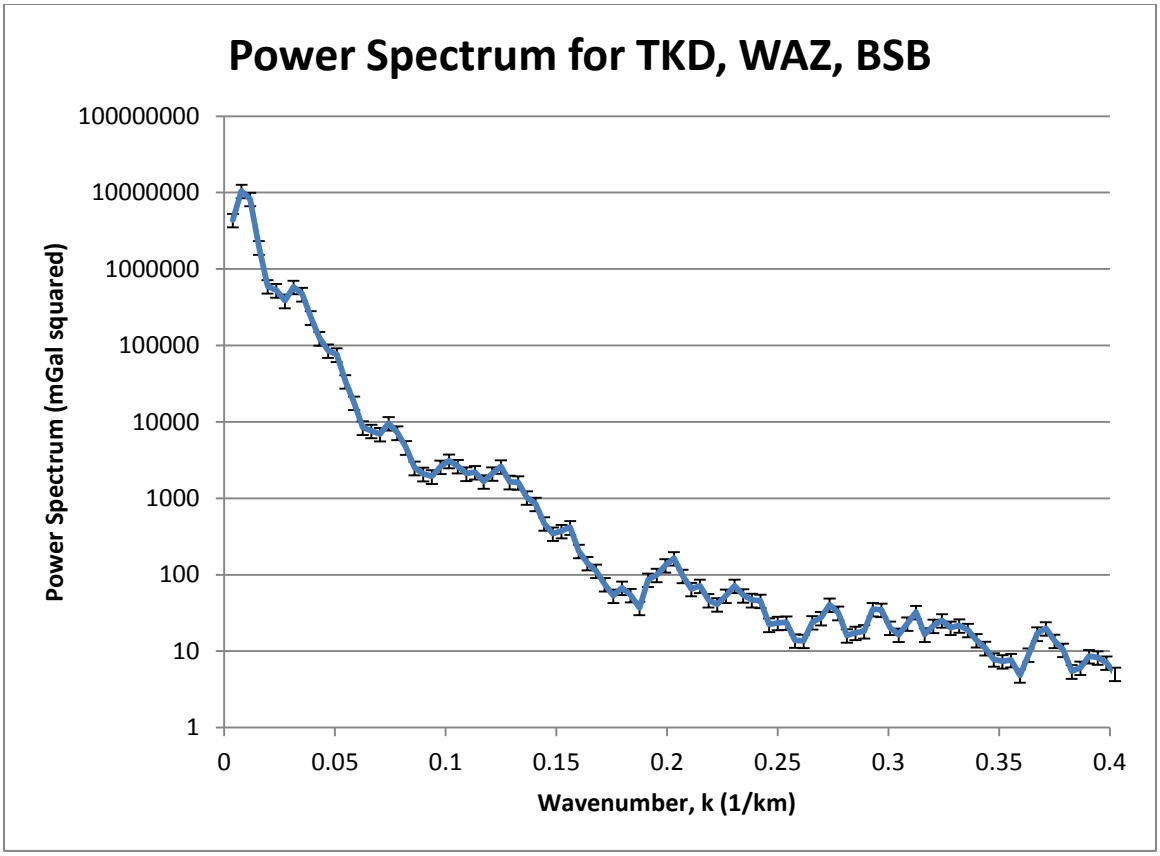

Figure 6.1: *The power spectrum from the Ross Ice Shelf end of TKD to the opposing end at BSB with BST.*

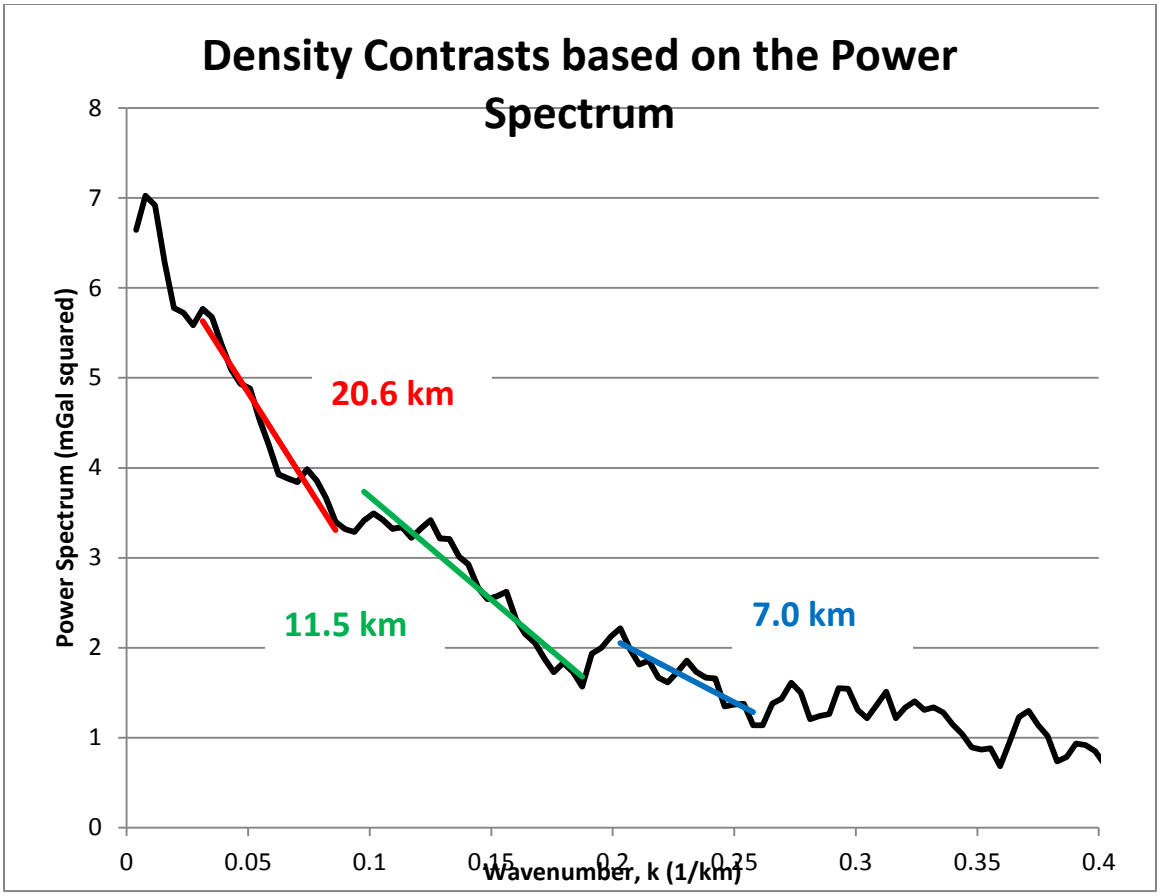

Figure 6.2: *The power spectrum from the Ross Ice Shelf end of TKD to the opposing end at BSB, including BST crust, and the line segments are in red, green, and blue.*

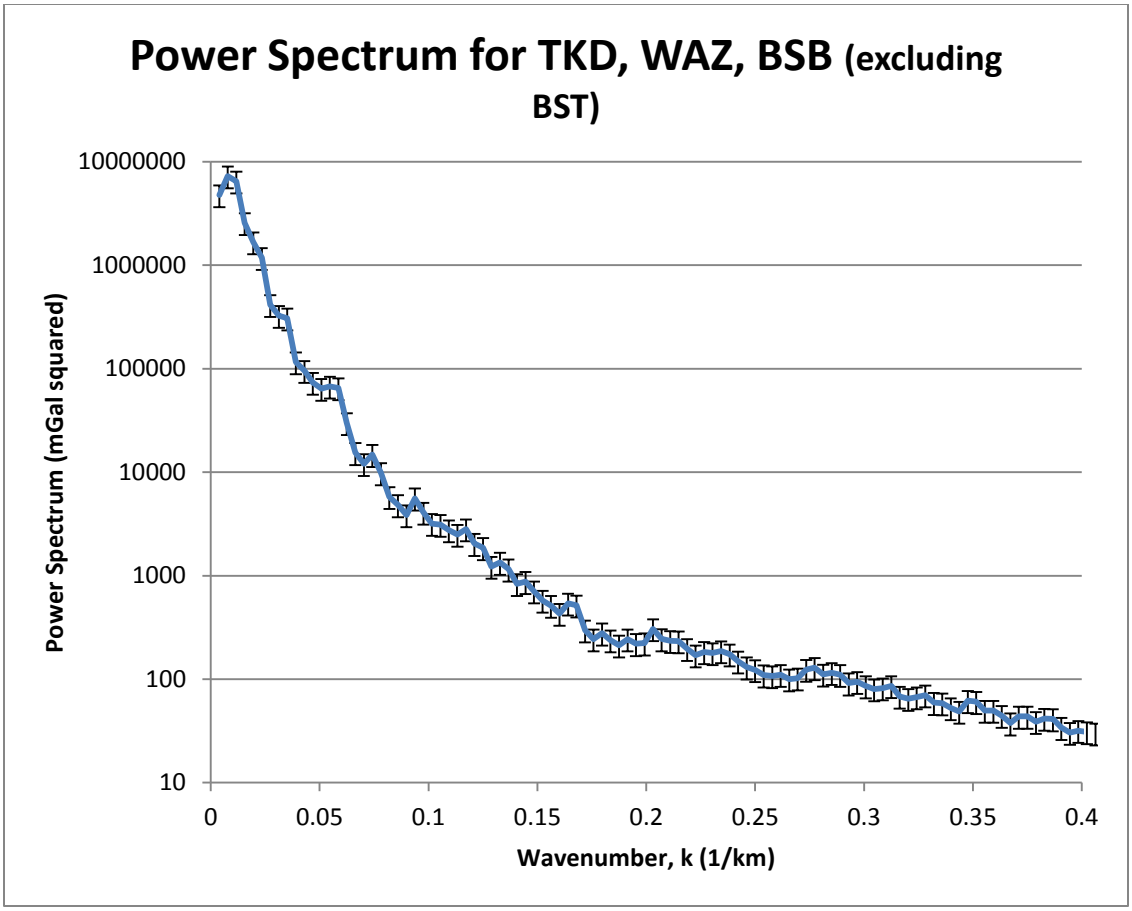

Figure 6.3: *The power spectrum from the Ross Ice Shelf end of TKD to the opposing end at BSB without BST.*

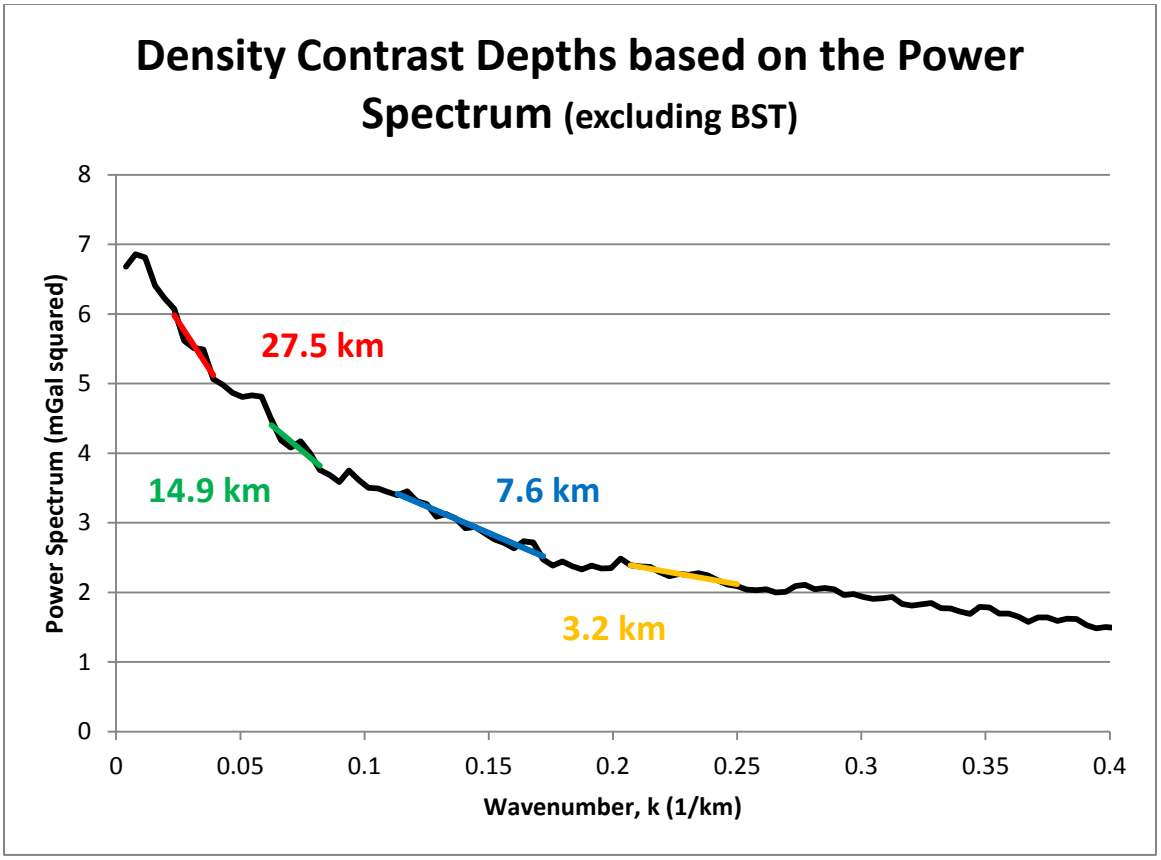

Figure 6.4: *The power spectrum from the Ross Ice Shelf end of TKD to the opposing end at BSB, without BST, and the line segments are in red, green, blue, and yellow.*

Chapter 7

Summary, Conclusions, and Further Work

7.1 Summary

A gravity study was carried out over West Antarctica, specifically on the Siple Coast focusing on Bindschadler Ice Stream and the boundaries of both MacAyeal and Kamb Ice Streams. The data were collected in an airborne survey between 1994-1997, by the UTIG research group. The data were processed to remove the vertical and horizontal accelerations, the Eötvös effect, and the theoretical gravity. The results gave the free-air gravity anomalies with RMS values that were in general better than previous analysis of the data. These free-air gravity data were then leveled with GOCE satellite gravity to match the rest of the region. The airborne gravity data retained their short wavelength, high frequency signals and took on the long wavelength, low frequency signal of the GOCE gravity. The Bouguer disturbance was calculated using a FORTRAN 90 program FA2BOUG. A power spectrum was calculated on the Bouguer disturbances in order to locate the density boundaries in the lithosphere

7.2 Conclusions

The new gravity data reduction techniques retain the original errors in the data, without introducing new errors due to line leveling. In comparison to previous studies

with similar data sets (e.g. Diehl, 2008), this reduction retains high frequency content which, in the Bouguer and power spectrum analyses, can be used to identify small scale features and near surface density contrasts. The improved reduction also demonstrates that simple corrections – vertical and horizontal accelerations, Eötvös, and theoretical gravity – are sufficient to match RMS values ($\leq$ 2.98 mGal) achieved previously by including line leveling.

The Bouguer analysis shows distinct positive anomalies, possible portions of sedimentary basins which match previous studies (Bell et al., 2006) and a general trend of less-negative Bouguer disturbances in the lithosphere towards the Ross Ice Shelf. This less-negative trend is consistent with decreasing distance from the Transantarctic Mountains. Since sedimentary basins likely control the inland extent of ice streams, identifying their boundaries is essential to characterizing ice streams and their possible future behavior.

While the Bouguer disturbance map is dominated by crustal signal, the power spectrum analysis, when Bentley Subglacial Trench is excluded from the analysis, identifies a density contrast at 3.2 km. Not only are sedimentary basins being identified in the region by the free-air gravity data and Bouguer analysis, the power spectrum also implies them. This shallow density contrast also supports the retention of high frequency, short wavelength content in the data.

The power spectrum identified a density contrast at the ice-bed interface, an upper density anomaly, a mid-crustal boundary, and the Moho. The differing crustal thickness

from spectral analysis also shows the character and extent of the West Antarctic Rift System, the northern flank of which extends out from Marie Byrd Land and into the survey area. Bindschadler Ice Stream is located on the WARS rift floor and MacAyeal Ice Stream sits on the rift flank. The location of the thicker crust under the northern part of Bindschadler – that is, distal from the Bentley Subglacial Trench – of 27.5 km, versus the seismically defined crustal thickness of 25 km on the southern flank of Marie Byrd Land could help with defining the extent of the possible low density mantle under Marie Byrd Land (Winberry and Anandakrishnan, 2004). The differing crustal thickness at the rift floor (27.5 km this study) and the northern rift flank (25 km, Winberry and Anandakrishnan, 2004) also imply different types of isostatic compensation: Airy for the rift floor (a thicker crustal root) and Pratt for the rift flank (the proposed low density mantle).

7.3 FURTHER WORK

The combination of the Bouguer anomalies and the crustal density boundaries can now be used to complete an inversion to locate the size and depth of the proposed sedimentary basins. Continued crustal structure studies in the Siple Coast would lead to better understanding of the crustal structure and isostatic compensation.

Bibliography

Achauer, Ulrich and Frédéric Masson. 2002. Seismic tomography of continental rifts revisited: from relative to absolute heterogeneities: *Tectonophysics* **358**, p. 17-37.

Alley, R. B. 1993. In search of ice-stream sticky spots: *Journal of Glaciology* **39**, p. 447-454.

Alley, R. B., D. D. Blankenship, C. R. Bentley, and S. T. Rooney. 1986. Deformation of till beneath Ice Stream B, West Antarctica: *Nature* **322**, p. 57-59.

Alley, R. B., D. D. Blankenship, C. R. Bentley, S. T. Rooney. 1987. Till beneath Ice Stream B 3. Till deformation: Evidence and implications: *Journal of Geophysical Research* **92**(B9), p. 8,921-8,929.

Alley, R. B., S. Anandakrishnan, C. R. Bentley, and N. Lord. 1994. A water-piracy hypothesis for the stagnation of Ice Stream C, Antarctica: *Annals of Glaciology*, **20**, p. 187-194.

Anandakrishnan, S. and J. P. Winberry. 2004. Antarctic subglacial sedimentary layer thickness from receiver function analysis: *Global and Planetary Change* **42**, p. 167-176.

Anandakrishnan, S. and R. B. Alley. 1997. Stagnation of Ice Stream C, West Antarctica by water piracy: *Geophysical Research Letters* **24**(3), p. 265-268.

Anandakrishnan, S., D. D. Blankenship, R. B. Alley, and P. L. Stoffa. 1998. Influence of subglacial geology on the position of a West Antarctic ice stream from seismic observations: *Nature* **394**, p. 62-65.

Anandakrishnan, Sridhar. 2003. Dilatant till layer near the onset of streaming flow of ice stream C, West Antarctica, determined by AVO (amplitude vs. offset) analysis: *Annals of Glaciology* **36**, p.283-286.

Banerjee, P. 1998. Gravity measurements and terrain corrections using a digital terrain model in the NW Himalaya: *Computers & Geosciences* **24**(10), p. 1009–1020.

Behrendt, John C. 1999. Crustal and lithospheric structure of the West Antarctic Rift System from geophysical investigations – a review: *Global and Planetary Change* **23**, p. 25-44.

Bell Aerospace. 1979. Operation and maintenance manual for gravity sensor subsystem BGM-3 (S/N 206 and subs.): *Report 6109-954026*: Buffalo, New York, Bell Aerospace Textron.

Bell, R. E., D. D. Blankenship, C. A. Finn, D. L. Morse, T. A. Scambos, J. M. Brozena, and S. M. Hodge. 1998. Influence of subglacial geology on the onset of a West Antarctic ice stream from aerogeophysical observations: *Nature* **394**, p.58-62.

Bell, R. E., M Studinger, G. Karner, C. A. Finn, and D. D. Blankenship. 2006. Identifying major sedimentary basins beneath the West Antarctica Ice Sheet from aeromagnetic data analysis. *in* Fütterer, Dieter K., Detlef Damaske, Georg Kleinschmidt, Hubert Miller, and Franz Tessensohn (eds). *Antarctica Contributions to Global Earth Science*: Berlin, Springer-Verlag, p. 117-122.

Bell, R. E., V. A. Childers, R. A. Arko, D. D. Blankenship, and J. M. Brozena. 1999. Airborne gravity and precise positioning for geologic applications: *Journal of Geophysical Research* **104**(B7), p. 15,281-15,292.

Bentley, C. R. 1987. Antarctic ice streams: a review: *Journal of Geophysical Research* **92**(B9), p. 8843-8858.

Bialas, Robert W., W. Roger Buck, Michael Studinger, and Paul G. Fitzgerald. 2007. Plateau collapse model for the Transantarctic Mountains – West Antarctic Rift System: Insights from numerical experiments: *Geology* **35**(8), p. 687-690.

Bindschadler, R. and P. Vornberger. 1998. Changes in the West Antarctic ice sheet since 1963 from declassified satellite photography: *Science* **279**(5351), p. 689-692.

Bingham, Robert G., Fausto Ferraccioli, Edward C. King, Robert D. Larter, Hamish D. Pritchard, Andrew M. Smith, and David G. Vaughan. 2012. Inland thinning of West Antarctic Ice Sheet steered along subglacial rifts: *Nature* **487**, p. 468-471.

Blankenship, D. D., C. R. Bentley, S. T. Rooney, and R. B. Alley. 1986. Seismic measurements reveal a saturated porous layer beneath an active Antarctic ice stream: *Nature* **322**, p. 54-57.

Blankenship, D. D., C. R. Bentley, S. T. Rooney, and R. B. Alley. 1987. Till beneath ice stream B: 1. Properties derived from seismic travel times: *Journal of Geophysical Research* **92**, p.8903-8911.

Blankenship, D. D., D. L. Morse, C. A. Finn, R. E. Bell, M. E. Peters, S. D. Kempf, S. M. Hodge, M. Studinger, J. C. Behrendt, and J. M. Brozena. 2001. Geologic controls

on the initiation of rapid basal motion for West Antarctic ice streams: A geophysical perspective including new airborne radar sounding and laser altimetry results. *in* Alley, R. B. and R. A. Bindschadler (eds). *The West Antarctic Ice Sheet: Behavior and Environment, Research Series* **77**: Washington, D. C., American Geophysical Union, p. 105-121.

Blankenship, Donald D., Robin E. Bell, Steven M. Hodge, John M. Brozena, John C. Behrendt, and Carol A. Finn. 1993. Active volcanism beneath the West Antarctic ice sheet and implications for ice-sheet stability: *Nature* **361**, p. 526-529.

Bradshaw, J. D. 1989. Cretaceous geotectonic patterns in the New Zealand region: *Tectonics* **8**, p. 803-820.

Bullard, E. C. 1936. Gravity measurements in East Africa: *Philosophical Transactions of the Royal Society, London* **235**, p. 445-534.

Cande, S. C., J. M. Stock, R. D. Miller, and T. Ishihara. 2000. Cenozoic motion between East and West Antarctica: *Nature* 4**04** (6775), p. 145-150.

Childers, Vicki A., Robin E. Bell, and John M. Brozena. 1999. Airborne gravimetry: An investigation of filtering: *Geophysics* **64**(1), p. 61-69.

Cooper, A. K. and F. J. Davey. 1987. Structure of extensionally rifted crust beneath the western Ross Sea and Iselin Bank, Antarctica, from sonobuoy seismic data. *in* Cooper, A. K. and F. J. Davey (eds). *The Antarctic Continental Margin: Geology and Geophysics of the Western Ross Sea, Earth Science Series* **5B**, Houston, Texas, Circum-Pacific Council for Energy and Mineral Resources, p. 93-118.

Dalziel, I. W. and D. H. Elliot. 1982. West Antarctica: Problem child of Gondwanaland: *Tectonics* **1**, p. 3-19.

Dalziel, I. W. D. and L. A. Lawver. 2001. The lithospheric setting of the West Antarctic Ice Sheet. *in* R. B. Alley and R. A. Bindschadler (eds). *The West Antarctic Ice Sheet: Behavior and Environment*: Washington, D. C., American Geophysical Union, p. 29-44.

Dalziel, Ian W. D. 1992. Antarctica; A tale of two supercontinents?: *Annual Review of Earth and Planetary Sciences* **20**, p. 501-526.

Dalziel, Ian W. D. 2006. On the extent of the active West Antarctic Rift System. *Terra Antartica Reports* **12**, p. 193-202.

Diehl, Theresa M. 2008. Gravity Analyses for the Crustal Structure and Subglacial Geology of West Antarctica, Particularly Beneath Thwaites Glacier [Ph. D. thesis]: Austin, The University of Texas at Austin, pp. 171.

Diehl, Theresa M., John W. Holt, Donald D. Blankenship, Duncan A. Young, Tom A Jordan, and Fausto Ferraccioli. 2008. First airborne gravity results over the Thwaites Glacier catchment, West Antarctica: *Geochemistry Geophysics Geosystems* **9**, Q04011, pp. 10.

Doake, C. S. M., H. F. J. Corr, A. Jenkins, K. Makinson, K. W. Nicholls, C. Nath, A. M. Smith, and D. G. Vaughan. 2001. Rutford Ice Stream, Antarctica. *in* Alley, R. B. and R. A. Bindschadler (eds). *The West Antarctic Ice Sheet: Behavior and Environment, Research Series* **77**: Washington, D. C., American Geophysical Union, p. 221-235.

Engelhardt, H. and B. Kamb. 1998. Basal sliding of ice stream B, West Antarctica: *Journal of Glaciology* **44**(147), p. 233-230.

Engelhardt, H., N. Humphrey, B. Kamb, and M. Fahnstock. 1990. Physical conditions at the base of a fast flowing Antarctic ice stream: *Science* **248**, p. 57-59.

Engelhardt, Hermann. 2004. Ice temperature and high geothermal flux at Siple Dome, West Antarctica, from borehole measurements: *Journal of Glaciology* **50**(169), p. 251-256.

Epanechnikov, V. A. 1969. Nonparametric estimation of a multidimensional probability density: *Theory of Probability and its Applications* **14**(1), p. 153-158.

European Space Agency. 2010. GOCE - ESA's Gravity Mission: *An ESA Communications Production* **BR-285**, pp. 20.

Fairhead, J. D. and C. S. Okereke. 1988. Depths to major density contrasts beneath the West African rift system in Nigeria and Cameroon based on the spectral analysis of gravity data: *Journal of African Earth Science* **7**, p. 769-777.

Featherstone, Will. 1995. On the use of Australian geodetic datums in gravity field determination: *Geomatics Research Australia* **62**, p. 17-36.

Fitzgerald, P. G., M. Sandiford, P. J. Barrett, and A. J. W. Gleadow. 1987. Asymmetric extension associated with the uplift and subsidence in the Transantarctic Mountains and Ross Sea Embayment: *Earth and Planetary Science Letters* **81**, p. 67-78.

Forsberg, R., 1985. Gravity field terrain effect computations by FFT: *Bulletin Géodesique* **59**, p. 342–360.

Fox Maule, Cathrine, Michael E. Purucker, Nils Olsen, and Klaus Mosegaard. 2005. Heat flux anomalies in Antarctica revealed by satellite magnetic data: *Science* **309**, p. 464-467.

Fullea, J., M. Fernàndez, and H. Zeyen. FA2BOUG – A FORTRAN 90 code to compute Bouguer gravity anomalies from gridded free-air anomalies: Application to the Atlantic-Mediterranean transition zone: *Computers and Geosciences* **34**, p. 1665-1681.

Hackney, Ron and Will Featherstone. 2001. Are we misinterpreting gravity anomalies?, Chapman Conference on Exploration Geodynamics, Dunsborough, Western Australia, Abstracts.

Hamilton, Gordon S. 2002. Mass balance and accumulation rate across Siple Dome, West Antarctica: *Annals of Glaciology* **35**, p. 102-106.

Harlan, R. B. 1968. Eötvös corrections for airborne gravimetry: *Journal for Geophysical Research* **73**, p. 4675-4679.

Hättestrand, C. and A. P. Stroeven. 2002. A relict landscape in the centre of Fennoscandian glaciation: Geomorphological evidence of minimal Quaternary erosion: *Geomorphology* **44**, p. 127-143.

Hayford, J.F., and W. Bowie. 1912. The effect of topography and isostatic compensation upon the intensity of gravity: *Bulletin of the American Geographical Society* **44** (6), p. 464–465.

Hindmarsh, R. 1998. Ice-stream surface texture, sticky spots, waves and breathers: *Journal of Glaciology* **44**, p.589-614.

Holt, John W., Thomas G. Richter, Scott D. Kempf, David L. Morse, and Donald D. Blankenship. 2006. Airborne gravity over Lake Vostok and adjacent highlands of East Antarctica: *Geochemistry Geophysics Geosystems* **7**(11), Q11012, pp. 15.

Hughes, T. J. 1977. West Antarctic ice streams: *Reviews of Geophysics* **15**, p. 1-46.

Jacobel, R. W., T. A. Scambos, N. A. Nereson and C. F. Raymond. 2000. Changes in the margin of Ice Stream C, Antarctica: *Journal of Glaciology* **46**(152), p. 102-110.

Jankowski, E. J. and D. J. Drewry. 1981. The structure of West Antarctica from geophysical studies: *Nature* **291**, p. 17-21. doi: 10.1038/291017a0.

Jankowski, E. J., and D. J. Drewry. 1981. The structure of West Antarctica from geophysical studies: *Nature* **291**, p. 17-21.

Jordan, T., F. Ferraccioli, D. Vaughan, J. Holt, H. Corr, D. Blankenship, and T. Diehl. 2009. Aerogravity evidence for major crustal thinning under the Pine Island Glacier region (west Antarctica): *Geological Society of America Bulletin* **122**, p.714–726, doi:10.1130/B26417.1.

Joughin, I. and S. Tulaczyk. 2002. Positive mass balance of the Ross Ice Streams, West Antarctica: *Science* **295**, p.476-480.

Joughin, I. R., S. Tulaczyk, R. Bindschadler, and S. F. Price. 2002. Changes in West Antarctica ice stream velocities: Observation and analysis: *Journal of Geophysical Research* **107**(B11), p. 2289-2311.

Kamb, B. 2001. Basal zone of the West Antarctic ice streams and its role in lubrication of their rapid motion. *in* R. B. Alley and R. A. Bindschadler (eds). *The West*

Antarctic Ice Sheet: Behavior and Environment: Washington, D. C., American Geophysical Union, p. 157-199.

Karner, G. D. and A. B. Watts. 1983. Gravity anomalies and flexure of the lithosphere at mountain ranges: *Journal of Geophysical Research* **88**, p. 10,449-10,477.

LaCoste, L. J. B. 1967. Measurement of gravity at sea and in the air: *Reviews of Geophysics* **5**, p. 477-526.

LaFehr, T. R. 1991a. Standardization in gravity reduction: *Geophysics* **56**(8), p. 1170-1178.

LaFehr, T.R., 1991b. An exact solution for the gravity curvature (Bullard B) correction: *Geophysics* **56**, p. 1178–1184.

Lawrence, Jesse F., Douglas A. Wiens, Andrew A. Nyblade, Sridhar Anandakrishnan, Patrick J. Shore, and Donald Voigt. 2006a. Crust and upper mantle structure of the Transantarctic Mountains and surrounding regions from receiver functions, surface waves, and gravity: Implications for uplift models: *Geochemistry Geophysics Geosystems* **7**(10), doi: 10.1029/2006GC001282.

Lawrence, Jesse F., Douglas A. Wiens, Andrew A. Nyblade, Sridhar Anandakrishnan, Patrick J. Shore, and Donal Voigt. 2006b. Upper mantle thermal variations beneath the Transantarctic Mountains inferred from teleseismic S-wave attenuation: *Geophysical Research Letters* **33**, L03303, doi: 10.1029/2005GL024516.

LeMasurier, W. E. and D. C. Rex. 1990. Late Cenozoic volcanism on the Antarctic Plate: An overview. *in* LeMasurier W.E. and J. W. Thomson (eds). *Volcanoes of the Antarctic Plate and Southern Oceans, Antarctic Research Series* **48**: Washington, D. C., American Geophysical Union, p. 1-17.

LeMasurier, W. E., Y. Kawachi, D.C. Rex, and F.A. Wade. 1990. Marie Byrd Land. *in* LeMasurier W.E. and J. W. Thomson (eds). *Volcanoes of the Antarctic Plate and Southern Oceans, Antarctic Research Series* **48**: Washington, D. C., American Geophysical Union, p. 147-256.

Li, Xiong and Hans-Jürgen Götze. 2001. Ellipsoid, geoid, gravity, geodesy, and geophysics: *Geophysics* **66**, p. 1660-1668.

Llubes, Muriel, Cédric Lanseau, and Frédérique Rémy. 2006. Relations between basal condition, subglacial hydrological networks and geothermal flux in Antarctica: *Earth and Planetary Science Letters* **241**, p. 655-662.

Luyendyk, B. P. 1995. Hypothesis for Cretaceous rifting of East Gondwana caused by subducted slab capture: *Geology* **23**, p. 373-376.

Luyendyk, B. P., D. S. Wilson, and C. S. Siddoway. 2003. Eastern margin of the Ross Sea Rift in Western Marie Byrd Land, Antarctica: Crustal structure and tectonic development: *Geochemistry, Geophysics, Geosystems* **4**(10), doi: 10.1029/2002GC000462.

McIntyre, N. F. 1985. The dynamics of ice-sheet outlets: *Journal of Glaciology* **31**(108), p. 99-107.

Morelli, Andrea and Stefania Danesi. 2003. Seismological imaging of the Antarctic continental lithosphere: a review: *Global and Planetary Change* **42**, p. 155-165.

Ng, Felix and Howard Conway. 2004. Fast-flow signature in the stagnated Kamb Ice Stream, West Antarctica: *Geology* **32**(6), p. 481-484.

Paterson, W. S. B. 1994. *The Physics of Glaciers*, 3rd Edition, Oxford, Pergamon, p. 301.

Paulsen, Timothy S. and Terry J. Wilson. 2010. Evolution of Neogene volcanism and stress patterns in the glaciated West Antarctica Rift, Marie Byrd Land, Antarctica: *Journal of the Geological Society London* **167**, p. 401-416.

Peters, Leo E, Sridhar Anandakrishnan, Richard B. Alley, J. Paul Winberry, Donal E. Voigt, Andrew M. Smith, and David L. Morse. 2006. Subglacial sediments as a control on the onset and location of two Siple Coast ice streams, West Antarctica: *Journal of Geophysical Research* **111**, B01302, doi:10.1029/2005JB003766.

Retzlaff, R. and C. R. Bentley. 1993. Timing of stagnation of Ice Stream C, West Antarctica, from short-pulse radar studies of buried surface crevasses: *Journal of Glaciology* **39**(133), p. 553-561.

Richter, T. G., J. W. Holt, D. D. Blankenship. 2001. Airborne gravity over East Antarctica: *in KIS 2001: Proceedings of the International Symposium on Kinematic Systems in Geodesy, Geomatics and Navigation*, Banff, Alberta, p. 576-585.

Rooney, S. T., D. D. Blankenship, R. B. Alley, and C. R. Bentley. 1991. Seismic refraction experiments of crustal structure in West Antarctica. *in* McKenzie, G. D. (ed). *Gondwana Six: Structure, Tectonics, and Geophysics, Geophysical Monogram Series* **40**: Washington, D. C., American Geophysical Union, p. 1-7.

Rooney, S. T., D. D. Blankenship, R. B. Alley, and C. R. Bentley. 1987. Till beneath Ice Stream B 2. Structure and continuity: *Journal of Geophysical Research* **92**(B9), p. 8,913-8,920.

Rooney, S. T., D. D. Blankenship, R. B. Alley, and C. R. Bentley. 1991a. Seismic reflection profiling of a sediment-filled graben beneath ice stream B, West Antarctica, *in* Thomson, M. R. A., J. A. Crane, and J. W. Thomson (eds). *Geological Evolution of Antarctica*, New York, Cambridge University Press, p. 261– 265.

Roult, G. and D. Rouland. 1994. Antarctica I; Deep structure investigation inferred from seismology; a review: *Physics of the Earth and Planetary Interiors* **84**, p. 15-32.

Schoof, Christian. 2001. Ice sheet grounding line dynamics: steady state, stability, and hysteresis: *Journal of Geophysical Research* **112**, F03S27, pp. 19.

Schopf, J. M. 1969. Ellsworth Mountains: position in West Antarctica due to sea floor spreading: *Science* **164**, p. 63-66.

Sengör, A. M. Celal and Kevin Burke. 1978. Relative timing of rifting and volcanism on Earth and its tectonic implications: *Geophysical Research Letters* **5**(6), p. 419-421.

Shabtaie, S., C. R. Bentley, R. A. Bindschadler, and D. R. MacAyeal. 1988. Mass-balance studies of Ice Streams A, B, and C, West Antarctica, and possible surging behavior of Ice Stream B: *Annals of Glaciology* **11**, p. 137-149.

Shapiro, Nikolai M. and Michael H. Ritzwoller. 2004. Inferring surface heat flux distributions guided by a global seismic model: particular application to Antarctica: *Earth and Planetary Science Letters* **233**, p. 213-224.

Siddoway, C. S. 2008. Tectonics of the West Antarctica Rift System: New light on the history and dynamics of distributed intracontinental extension. *in* Cooper, A. K., P. J. Barrett, H. Stagg, B. Storey, E. Stump, W. Wise and the 10th ISAES editorial team (eds). *Antarctica: A Keystone in a Changing World*. Proceedings of the 10th International Symposium on Antarctica Earth Sciences: Washington, D. C., The National Academies Press. p. 91-114. doi: 10.3133/of2007-1047.kp09.

Siegert, Martin J., Justin Taylor, and Antony J. Payne. 2005. Spectral roughness of subglacial topography and implications for former ice-sheet dynamics in East Antarctica: *Global and Planetary Change* **45**, p. 249-263.

Siegert, Martin J., Justin Taylor, Antony J. Payne, and Bryn Hubbard. 2004. Macro-scale bed roughness of the Siple Coast ice streams in West Antarctica: *Earth Surface Processes and Landforms* **29**, p. 1591-1596.

Skou, N. and F. Sondergaard. 1976. *Radioglaciology: A 60 MHz Ice Sounder System, Report* **R169**: Lyngby, Electromagnetics Institute, Technical University of Denmark, 124pp.

Smith, A. M. 1997. Basal conditions on Rutford Ice Stream, West Antarctica, from seismic observations: *Journal of Geophysical Research* **102**, p. 543-552.

Spector, A. and F. S. Grant. 1970. Statistical models for interpreting aeromagnetic data: *Geophysics* **35**, p. 293-302.

Stokes, Chris R. and Chris D. Clark. 2001. Paleo-ice streams: *Quaternary Science Reviews* **20**, p. 1437-1457.

Storey, B. C., P. T. Leat, S. D. Weaver, R. J. Pankhurst, J. D. Bradshaw, and S. Kelley. 1999. Mantle plumes and Antarctica-New Zealand rifting: Evidence from mid-Cretaceous mafic dykes: *Journal of the Geological Society of London* **156**, p. 659-671.

Studinger, Michael, Robin E. Bell, Donald D. Blankenship, Carol A. Finn, Robert A. Arko, David L. Morse, and Ian Joughin. 2001. Subglacial sediments: A regional geological template for ice flow in West Antarctica: *Geophysical Research Letters* **28**(18), p. 3493-3496.

Studinger, Michael, Robin E. Bell, W. Roger Buck, Garry D. Karner, and Donald D. Blankenship. 2004. Sub-ice geology inland of the Transantarctic Mountains in light of new aerogeophysical data: *Earth and Planetary Science Letters* **220**, p. 391-408.

ten Brink, Uri S., Ron J. Hackney, Stephen Bannister, Tim A. Stern, and Yizhaq Makovsky. 1997. Uplift of the Transantarctic Mountains and the bedrock beneath the East Antarctic ice sheet: *Journal of Geophysical Research* **102**(B12), p. 27,603-27,621.

Tenzer, R., A. Ellmann, P. Novák, and P. Vajda. 2008. The Earth's gravity field components of the differences between gravity disturbances and gravity anomalies. *in* Sideris, M. G. (ed). *Observing our Changing Earth, International Association of Geodesy Symposia* ***133****(2)*: Berlin, Springer-Verlag, p. 155-159.

Tessensohn, F. and G. Worner. 1991. The Ross Sea rift system, Antarctica: Structure, evolution, and analogs. *in* Thompson, M. R. A., J. A. Crame, and J. W. Thompson (eds). *Geological Evolution of Antarctica*: New York, Cambridge University Press, p. 273-278.

Truffer, Martin and Keith A. Echelmeyer. 2003. Of isbrae and ice streams: *Annals of Glaciology* **36**, p. 66-72.

Tulaczyk, S., B. Kamb, R. P. Sherer, and H. F. Engelhardt. 1998. Sedimentary processes at the base of a West Antarctic ice stream: Constraints from textural and compositional properties of subglacial debris: *Journal of Sedimentary Research* **68**(3), p. 487-496.

Vaughan, D. G., A. M. Smith, P. C. Nath, and E. le Meur. 2003. Acoustic impedence and basal shear stress beneath four Antarctic ice streams: *Annals of Glaciology* **36**, p.225-232.

Weaver, S. D., B. Storey, R. J. Pankhurst, S. B. Mukasa, V. J. Divenere, and J. D. Bradshaw. 1994. Antarctica-New Zealand rifting and Marie Byrd Land lithosphere magmatism linked to ridge subduction and mantle plume activity: *Geology* **22**, p. 811-814.

Wessel, P. and W. H. F. Smith. 1998. New, improved version of Generic Mapping Tools released: *Eos Transactions* **79**(47), p. 579.

Whillans, I. M. and C. J. van der Veen. 1993. Controls on changes in the West Antarctic Ice Sheet. *in* Peltier, W. R. (ed). *Ice in the Climate System*, NATO ASI Service, Series I, **12**, p. 47054.

Winberry, J. Paul and Sridhar Anandakrishnan. 2004. Crustal structure of the West Antarctic rift system and Marie Byrd Land hotspot: *Geology*, **32**(11), p. 977-980.